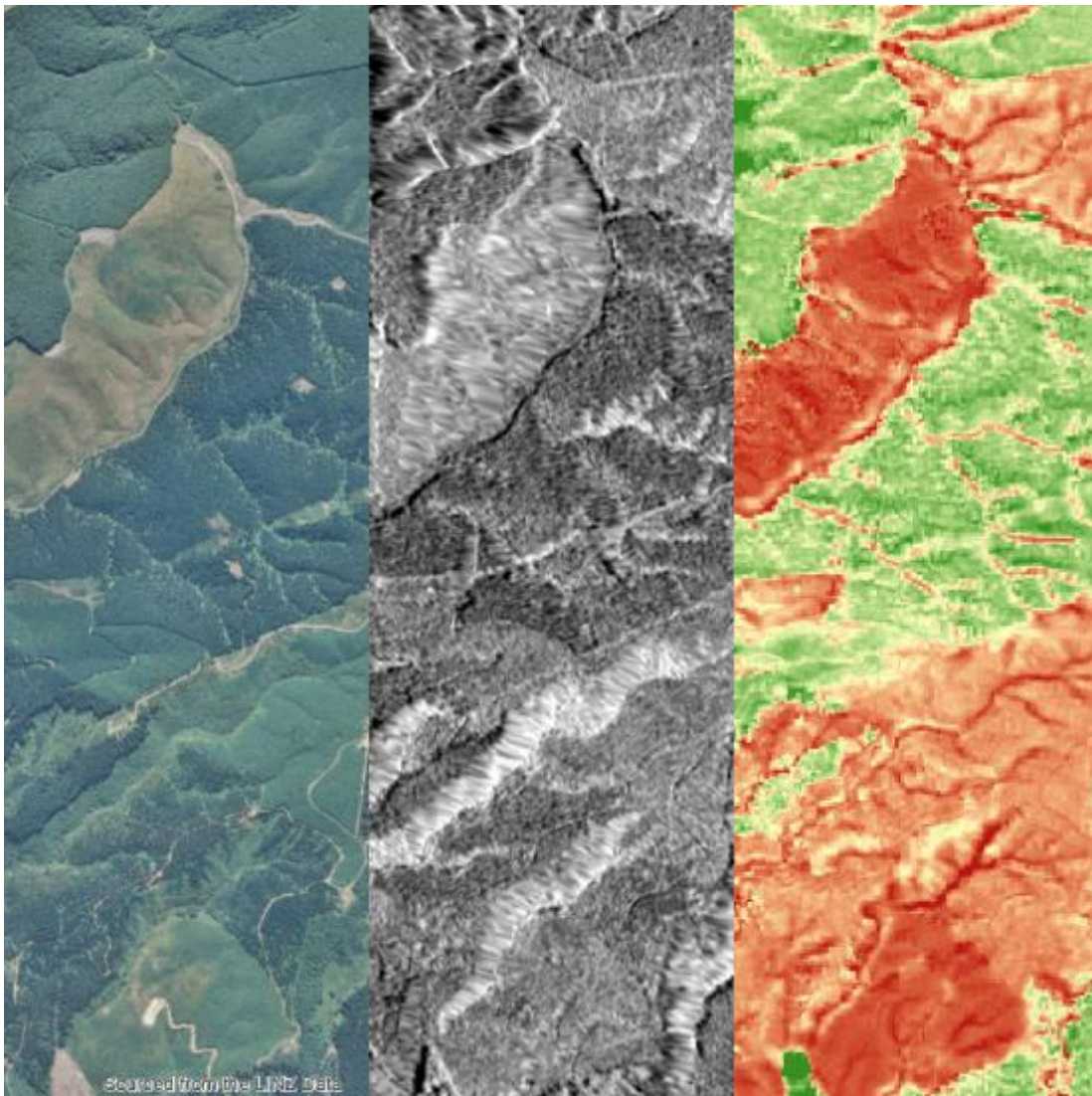


Comparison of TanDEM-X InSAR data and high-density ALS for the prediction of forest inventory attributes in plantation forests with steep terrain

Ellen Mae Leonardo, Michael S. Watt, Grant D. Pearse, Jonathan P. Dash & Henrik J. Persson



Report information sheet

| | |
|------------------------------|---|
| Report title | Comparison of TanDEM-X InSAR data and high-density ALS for the prediction of forest inventory attributes in plantation forests with steep terrain |
| Authors | Ellen Mae Leonardo, Michael S. Watt, Grant D. Pearse, Jonathan P. Dash, Henrik J. Persson |
| Client | Forest Owners Association |
| Signed off by | Michael Watt |
| Date | June 2019 |
| Intellectual property | © New Zealand Forest Research Institute Limited. All rights reserved. Unless permitted by contract or law, no part of this work may be reproduced, stored or copied in any form or by any means without the express permission of the New Zealand Forest Research Institute Limited (trading as Scion). |
| Disclaimer | <p>The information and opinions provided in the Report have been prepared for the Client and its specified purposes. Accordingly, any person other than the Client uses the information and opinions in this report entirely at its own risk. The Report has been provided in good faith and on the basis that reasonable endeavours have been made to be accurate and not misleading and to exercise reasonable care, skill and judgment in providing such information and opinions.</p> <p>Neither Scion, nor any of its employees, officers, contractors, agents or other persons acting on its behalf or under its control accepts any responsibility or liability in respect of any information or opinions provided in this Report.</p> |

Executive summary

The problem

Aerial Laser Scanning (ALS or LiDAR) is an extremely valuable form of remote sensing for estimating forest inventory attributes, as well as extracting accurate terrain information, and producing canopy surface models for a given area of interest. However, it is very expensive to capture at ~ \$3-\$15/ha and can have lengthy turn-around times due to flight delays, provider scheduling conflicts, and long processing times.

Satellite based Interferometric Synthetic Aperture Radar (InSAR) is an active sensor that can provide continuous global coverage with the quality of the acquisition largely independent of cloud cover and solar illumination conditions. InSAR provides a much more cost-effective potential solution at ~ \$0.16/ha and has been successfully used to characterise forest inventory attributes and to provide accurate terrain information in other countries. New Zealand forestry provides a unique challenge due to the often mountainous landscape and the dense canopy of mature plantation forestry which is difficult for radar to penetrate.

Client initiatives

Despite the wide use of satellite based InSAR within the northern hemisphere we are unaware of any research that has used these data to predict key forest inventory biophysical variables or to characterise the digital terrain model (DTM) within New Zealand forests.

This project

InSAR and ALS data was collected from Geraldine Forest, which is a 62 km² plantation, predominantly composed of *Pinus radiata* D. Don, that is located on rolling to very steep topography in Canterbury. These data were combined with an extensive set of plot measurements, from which mean top height (H), basal area (G), stem density (N) and total stem volume (TSV) were extracted. Using these data, the objectives of this study were to (i) compare model precision for these four biophysical variables using metrics derived from InSAR and ALS data, (ii) identify the importance of base metrics, metrics derived from the canopy height model (CHM) and textural metrics within these models and (iii) quantify how slope influences bias and precision of the base surfaces and the final models.

Precision of these models was compared using the co-efficient of determination (R^2), root mean square error (RMSE) and the RMSE expressed as a percentage of the mean value for each biophysical variable (RMSE_%)

Key results

Random Forest models developed using ALS data were substantially more precise than those developed from InSAR for H ($R^2 = 0.86$ vs. 0.60 ; RMSE_% = 5.47 vs. 10.8%), G ($R^2 = 0.56$ vs. 0.32 ; RMSE_% = 21.5 vs. 30.4%), N ($R^2 = 0.47$ vs. 0.09 ; RMSE_% = 32.3 vs. 43.2%), and TSV ($R^2 = 0.70$ vs. 0.41 ; RMSE_% = 19.4 vs. 30.7%). Although InSAR models were clearly less precise than ALS models, these models did provide a reasonable level of precision for H and TSV , which was significantly improved through inclusion of metrics from the mixed Canopy Height Model (CHM), derived from the radar Digital Surface Model (DSM) and ALS DTM. The mean errors (RMSE) associated with the InSAR DSM and DTM were, respectively, 4.58 and 8.09 m, and these errors increased markedly as slope increased. For instance, the RMSE for the DTM was 4.51 m for $10\text{--}20^\circ$ slopes and increased to 10.17 m for slopes ranging from $40\text{--}50^\circ$. Although the bias and precision of the underlying and derived InSAR surfaces (DTM, DSM and CHM) markedly deteriorated with increasing slope both bias and precision for the final InSAR models were invariant to slope.

Implications of results for the client

Although InSAR could not predict the four biophysical variables as precisely as ALS the predictions of two of the key variables *H* and *TSV* were likely to be of a sufficient precision for inventory purposes. Results also show that the DTM derived from InSAR was reasonably precise, particularly at slopes lower than 20°, for which the RMSE was ≤ 4.5 m. Given the large cost differential between InSAR and ALS (\$0.16/ha vs. \$3 – 15/ha) there may be applications where the lower cost of InSAR is a more important consideration than the greater precision afforded by ALS. These situations could include remote or scattered forest in which acquisition of ALS is not cost effective or repeat acquisitions for which the cost of the inventory does not justify an additional ALS acquisition.

Further work

Results from this study are likely to be conservative as this study was undertaken over a forest with very steep terrain and a key setting during image acquisition, Height of Ambiguity (HOA), was not optimised. Further research should investigate if precision gains in predictions of inventory variables are possible under acquisitions with optimised HOA. Predictions could also be improved through using an ascending and descending stereo pair to derive a digital surface model in which the effect of slope is minimised. Even if further improvements are not possible the precision demonstrated within this study does highlight the potential of InSAR as a valuable means of supplying an inexpensive DTM and a reasonably precise means of predicting key inventory metrics.

Comparison of TanDEM-X InSAR data and high-density ALS for the prediction of forest inventory attributes in plantation forests with steep terrain

Table of contents

| | |
|---|----|
| Executive summary | 3 |
| Introduction | 6 |
| Materials and methods | 8 |
| Study Area | 8 |
| Datasets | 8 |
| Processing of InSAR and ALS predictive metrics | 10 |
| Data analysis | 12 |
| Results | 13 |
| Data range | 13 |
| Relationships between the ALS and Radar DTM, DSM and CHM | 14 |
| Correlations between biophysical variables and metrics derived from ALS and Radar | 17 |
| Models of biophysical variables | 17 |
| Discussion | 23 |
| Recommendations and conclusions | 26 |
| Acknowledgements | 26 |
| References | 27 |
| Appendix A | 30 |
| Appendix B | 31 |

Introduction

Forest managers require detailed inventory information to monitor crop health and damage, optimise silvicultural treatments, and estimate stand volume and value. Sample based methods that estimate biophysical variables of interest, such as height, volume, and stand density, have been traditionally used to supply this information at the stand level. However, the last two decades have seen a rapid increase in the availability of remotely sensed information which has become widely integrated into forest inventories, providing improvements in precision and a means of spatially predicting the variance in biophysical variables at a relatively fine resolution (Dash et al. 2015; Persson et al. 2017).

The integration of airborne laser scanning (ALS or LiDAR) into forest inventory, primarily through the area-based approach (ABA), is now accepted as the most accurate supplemental data source for characterising a wide range of biophysical variables (Rahlf et al. 2014; Wittke et al. 2019; Yu et al. 2015). The high cost of ALS is the key impediment to routine acquisition of this data. As a consequence, there has been considerable interest around the use of point clouds derived from digital aerial photogrammetry (DAP) for forest inventory that can be supplied at a lower cost. Although DAP has generally been shown to have a similar accuracy to ALS this technology does require a digital terrain model (DTM), which is often obtained from an earlier ALS survey (Goodbody et al. 2019).

Satellite-based information has also been widely investigated as an alternative to ALS for inventory purposes. Photogrammetric point clouds acquired from satellite offer a relatively precise alternative to ALS (e.g. Pearse et al. 2018; Persson 2016) but this method requires a DTM to normalise the resulting point cloud and acquisition is limited to cloud free conditions which makes frequent monitoring difficult particularly in tropical and maritime areas. In contrast, Synthetic Aperture Radar (SAR) is an active sensor that can provide continuous global coverage with the quality of the acquisition largely independent of cloud cover and solar illumination conditions. Over the last half-century, little research was focussed around the use of SAR for forest inventory as the precision of this method was limited due to issues around data quality, resolution, and signal saturation when estimating forest biophysical variables from backscatter intensity at shorter wavelengths (Dobson et al. 1992; Fransson 1999; Rignot et al. 1994).

However, over the last two decades there have been major advances in SAR-based techniques that go beyond the application of backscatter-based methods. Interferometric SAR (InSAR) has been widely investigated as a method that can be used for forest inventory. InSAR can be used to determine differences in elevation and generate a digital surface model (DSM) from the phase differences of two SAR images that are acquired from slightly different perspectives (Massonnet and Feigl 1998). This method provides two further observables in addition to radar backscatter, that describe the interferometric phase and coherence.

The accuracy of early forest applications of InSAR were often limited by temporal decorrelation that occurs when the SAR images forming the interferometric coherence are acquired at different times (Lavalle and Hensley 2015; Lee et al. 2013). The temporal decorrelation is closely connected to the wavelength of the SAR and to the scattering objects. Hence, InSAR works better for applications with relatively stable scatterers (e.g., buildings, volcanoes or glaciers). Vegetation and trees in the forest decorrelate within seconds at X- and C-band, while at longer wavelengths (L- and P-band), the decorrelation is less severe with repeat-pass configurations. The spaceborne SAR mission TanDEM-X operated by the German Aerospace Centre (Deutsches Zentrum für Luft- und Raumfahrt – (DLR)) heralded a new era in InSAR remote sensing. This mission uses two X-band SAR satellites, launched in 2007 and 2010, flying in close formation to acquire X-band InSAR images with single and dual polarizations at a very high resolution (Krieger et al. 2007). The simultaneous acquisition of images increases the correlation between the InSAR observables and forest variables as temporal decorrelation can be assumed to be negligible (Karila et al. 2019).

A growing body of research has shown that InSAR data from TanDEM-X provides reasonably precise estimates of forest biophysical variables. In almost all studies, ALS data has been used as a basis for comparison and, with a few exceptions (e.g. Persson and Fransson 2017), these studies show predictions of biophysical variables from InSAR to be less precise than those from ALS. More extensive comparisons have also shown that predictions from InSAR are

less precise than those derived from satellite photogrammetric point clouds (Yu et al. 2015) but that InSAR has a higher precision than radargrammetry (Rahlf et al. 2014; Yu et al. 2015). Despite this, predictions of forest biophysical variables from InSAR have often been found to be sufficiently precise for forest inventory purposes in some contexts. As a consequence, InSAR has been used to predict forest biomass and volume, with a reasonable degree of precision across the entire spatial extent of Sweden (Persson et al. 2017).

Interferometric SAR provides a number of variables that can be used to predict forest biophysical variables. Relationships between the complex coherence, which describes the correlation between two SAR images, and forest height or biomass have been demonstrated using TanDEM-X acquisitions (Askne et al. 2013; Askne et al. 1997; Kugler et al. 2014; Olesk et al. 2016; Soja et al. 2015b; Treuhaf et al. 2015). As the X-band scattering generally occurs at the top of the canopy (Le Toan et al. 1992), the normalised phase height (PH, but commonly known as the canopy height model, CHM) can be generated by removing the ground elevation, with the DTM usually generated from ALS. The CHM has been shown to be positively correlated to forest height and above ground biomass (Abdullahi et al. 2016; Persson et al. 2017; Persson and Fransson 2017; Solberg et al. 2013). Although much research has investigated the utility of InSAR phase, backscatter and coherence (hereafter denoted base outputs), with a few exceptions (e.g. Abdullahi et al. 2016), little research has investigated whether the addition of texture metrics, derived from the CHM, add to the precision of InSAR models.

Most research using InSAR has been undertaken within European and tropical forests. Forest types that have been studied include boreal forests, located in northern Europe and Canada (Askne et al. 2013; Askne and Santoro 2015; Askne et al. 2017; Chen et al. 2016; Karila et al. 2015; Olesk et al. 2016; Persson et al. 2017; Persson and Fransson 2017; Rahlf et al. 2014; Soja et al. 2015a; Solberg et al. 2013; Yu et al. 2015), natural or plantation forests located in the tropics (Gama et al. 2010; Hansen et al. 2015; Neeff et al. 2005; Puliti et al. 2017; Treuhaf et al. 2015) temperate forests in Germany (Abdullahi et al. 2016; Schlund et al. 2019) or a combination of these forest types (Kugler et al. 2014; Qi et al. 2019). Despite the wide use of InSAR from TanDEM-X within the northern hemisphere, we are unaware of any research that has used these data to predict forest biophysical variables within temperate plantations located in the Southern Hemisphere.

New Zealand plantation forests, which are mainly composed of *Pinus radiata* D. Don (radiata pine), constitute 90% of the 1.8 Million hectare plantation estate (NZFOA 2018). As a highly productive system, with relatively short rotation lengths, these plantations require continuous monitoring to provide managers with up-to-date information to plan management interventions and for operational planning. Although ALS surveys are increasingly used for plantation inventory within the larger estates, the use of InSAR is seen as an attractive option as this method could markedly reduce costs and allow more regular inventory updates across a larger portion of New Zealand's planted forests.

Within New Zealand, a significant proportion of plantations (39%) are located on sites with rolling to very steep topography that have mean slopes exceeding 15° (Watt et al. 2011). Topography, and the associated variations in aspect, are two of the key factors influencing the usability of InSAR data. Although both variables have been found to influence predictive precision of models describing biophysical variables (Rahlf et al. 2014), little research has examined the influence of these factors on the predictive precision of InSAR across slopes that range from flat and gently undulating to very steep. Further research is therefore required to understand the potential of InSAR for inventory purposes within New Zealand plantations and other countries that have a large proportion of their forests located on highly dissected terrain.

InSAR and ALS data was collected from Geraldine Forest, which is a moderate sized plantation, predominantly composed of *Pinus radiata* D. Don., that is located on rolling to very steep topography in the east of the South Island, New Zealand. These data were combined with an extensive set of plot measurements, from which mean top height (H), basal area (G), stem density (N) and total stem volume (TSV) were extracted. Using these data, the objectives of this study were to (i) compare model precision for these four biophysical variables using metrics derived from InSAR and ALS data, (ii) compare the importance of base metrics, metrics derived from the canopy height model (CHM) and textural metrics within these models, and (iii) quantify how slope influences bias and precision of the base surfaces and the final models.

Materials and methods

Study Area

The study was undertaken within the temperate Geraldine Forest (centred at latitude 44°5'S, longitude 171°4'W) located in the South Island, New Zealand (Fig. 1). The forest, which covers ca. 62 km², is located across terrain ranging from rolling to very steep, with slopes ranging from 0.04 – 67.0°. Elevations vary widely across the forest from 145 to 860 m with the highest points located in the northwest. The forest is predominantly composed of even aged stands of *P. radiata* that are managed for timber production and models were developed in this study for this species.

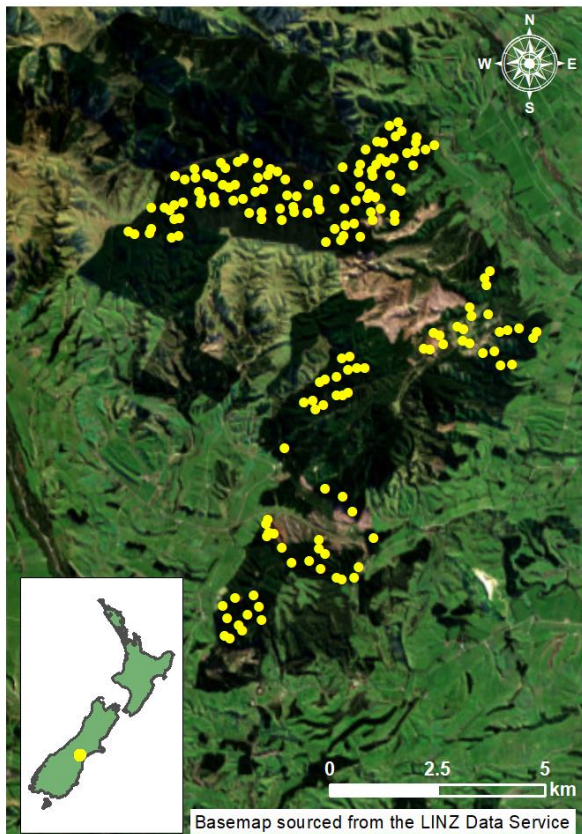


Figure 1: Study area with the field measurements at plot-level. The inset map shows the location of Geraldine Forest in New Zealand

Datasets

Remote Sensing Datasets

Table 1 summarises the key specifications for all remotely sensed datasets. With the primary objective of developing global digital elevation model (WorldDEM) products, the TanDEM-X (TDX) satellite was designed after the existing TerraSAR-X (TSX) satellite. Both have X-band SAR instruments. The TDX mission utilises two identical spacecraft that fly in a close formation made possible by assuming helix orbits. The two satellites never collide due to differences in the along-track direction, enabling them to be shifted and meet the minimum baseline requirements (i.e. 150 to 500 m) for generating a precise DEM (Zink et al. 2006). The mission (TSX and TDX together) provides a platform for collecting bistatic InSAR data with minimal temporal decorrelation, with one satellite transmitting and both satellites receiving the same signal.

Table 1: Product specifications for the ALS, InSAR, and the WorldDEM datasets.

| | ALS | InSAR | WorldDEM |
|------------------------|--|--|---|
| Description | Classified high density ALS | CoSSC bistatic data in raw format | Pre-processed DTM and DSM provided by Airbus in raster format |
| Sensor System | Reigl Q1560 scanner system onboard an aircraft | X-band radar sensor onboard TerraSAR-X and TanDEM-X satellites | |
| Date of Capture | June 13-14, 2016 | March 11, 2014 | |
| Resolution | 1 m | 5 m | 10.7 m |

A pair of TDX co-registered single-look complex (CoSSC) bistatic data with HH polarization (horizontally transmit, horizontally receive) was captured by the TDX mission overlooking Geraldine Forest on March 11, 2014. The images were acquired from a descending orbit, in StripMap (SM) mode. With an HH polarization, the InSAR was expected to penetrate slightly more than the vertical transmit/receive channel (Kugler et al. 2014; Perko et al. 2011). The single-look complex (SLC) resolution was 2.7 m in slant range and 3.3 m in azimuth with a pixel spacing of 1.8 m and 2.1 m, respectively. The mean scene incidence angle was 40.5°. Steep incidence angles decrease the height sensitivity and increase the penetration depth (Kugler et al. 2014). The overall incidence angle was suitable for forest height estimation, but the varying topography caused the local incidence angle to deviate from the mean. The height of ambiguity (HOA), which was 216 m, is related to the baseline and describes the height sensitivity of the interferometer. It describes the altitude difference that generates an interferometric phase change of $2\pi \times \text{Ambiguity}$. It relates to the baseline and system configuration as described below,

$$HOA = \frac{2\pi}{k_z} = \frac{\lambda R \sin\theta}{B_{\perp}}$$

where k_z is the vertical wave number, λ is the radar wavelength, R is the average distance to the satellites, θ is the average angle of incidence, and B_{\perp} is the perpendicular baseline.

Processed WorldDEM™ products of the first surface and bare Earth elevations, also known, respectively, as the DSM and DTM were also acquired from Airbus Intelligence. These global WorldDEM™ surfaces are derived from at least two acquisitions with differing HOA and for these surfaces the DTM is generated by filtering out the vegetation and buildings from the DSM (all carried out by Airbus). The scene that we used for manual processing was one of at least two scenes used for the constructing the WorldDEM™. The target specifications for the WorldDEM™ product include an absolute vertical accuracy of <10 m and a relative vertical accuracy (90% linear point to point error) of 2 m for slopes ≤ 20% and 4 m for slopes > 20% (Wessel 2016). Using ArcMap 10.6, both WorldDEM™ products were projected to New Zealand Transverse Mercator Projection (NZTM 2000) with a resulting spatial resolution of 10.7 m.

High-density ALS data was acquired from the study site on June 13–14, 2016 using a Reigl Q1560 scanner system. This scanner recorded an average pulse density of 21.1 pulses m⁻² using a pulse rate of 330 kHz and maximum scan angle of 14° off nadir. A detailed description of the ALS data is given in Pearse et al. (2018).

Field data

Plot measurements of diameter at breast height (DBH), total tree height, stem counts, as well as tree descriptions were collected from May to June 2016. Field plots were located throughout the forest using systematic sampling based on a grid with a randomised start point and orientation. The ground sampling unit was a circular bounded plot with a slope corrected area of 600 m². Plot centres were located using a Trimble Geo6/7 Series GNSS (Trimble Navigation Ltd., Sunnyvale CA, USA). These measurements served as input to a commercial forest yield prediction software package (YTGEN, Silmetra, Tokoroa, New Zealand) which was used to produce plot-level estimates for the four modelled forest biophysical attributes, namely, mean top height (H), basal area (G), stand density (N), and total stem volume (TSV). A detailed description of the methods used to calculate these values can be found in Pearse et al. (2018).

Field measurements were projected to dates that temporally coincided with the time of the InSAR (11 March 2014) and ALS captures (June 14, 2016) using a commercial forest growth model used by the forest manager for Geraldine forest. After discarding the plots in unproductive areas, those with incomplete measurements, and plots in which there was no data from the InSAR, a total of 171 plots were available for model development (Table 2).

Processing of InSAR and ALS predictive metrics

The InSAR predictive metrics were divided into four categories that included (1) base metrics, (2) CHM metrics, (3) textural metrics based on the Mixed CHM, and (4) textural metrics based on the Radar CHM as shown in Appendix 1. The ALS predictors were divided into three categories, that included (1) base metrics, (2) CHM metrics, and (3) textural metrics, all of which are summarised in Appendix 2. A flowchart showing the process by which each of these metric classes were generated is given in Figure 2 and the derivation of these predictors is described in more detail below in the following sections.

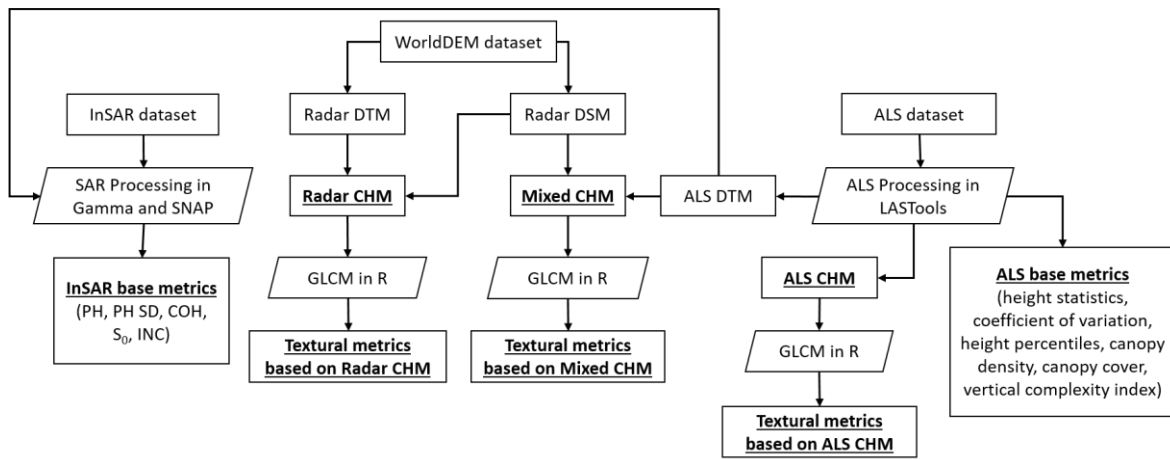


Figure 2. Simplified flowchart showing the derivation of the predictive metrics (bold and underlined) from the three source datasets: InSAR, WorldDEM, and ALS.

InSAR base metrics

The TanDEM-X data were processed using the software Gamma ver. 2016-12-07 (Gamma Remote Sensing AG) and Sentinel Application Platform (SNAP, ESA). One advantage of acquiring an interferometric pair of TanDEM-X data (consisting of one image s_i from each satellite j) was that the backscattering coefficient (S_0) could be computed from each acquisition pair, as well as the coherence (COH) and the interferometric phase (PH).

The calibration gain provided in the metadata for each acquisition (~ 50 dB) was subtracted from the multi-looked intensity images (β^0), before a radiometric normalization based on the pixel-area method was applied, as described in Frey et al. (2012) and Small (2011). One backscatter image per acquisition pair was then computed as the arithmetic mean of the two normalized S_0 images within the image pair.

An interferogram was derived with a spatial averaging of five looks in range and five looks in azimuth. This reduced the phase noise standard deviation by approximately a factor of five (Moreira et al. 2013). The interferogram was flattened by subtracting the ground phase, derived from the satellite orbit data and the ALS DTM. The flattened interferogram was adaptively filtered with a function based on the local fringe spectrum and using a coherence kernel of 3×3 pixels and a 16-pixel fast Fourier transform window (Goldstein and Werner 1998). The output phase was unwrapped by applying a minimum cost flow (MCF) phase unwrapping algorithm (Wegmüller et al. 2002). The unwrapped phase was converted to height using a phase-to-height sensitivity raster, which was generated from the differential interferometric phase and the orbital state vectors, using Gamma.

COH was estimated from the normalized interferogram and the multi-looked intensity images, using a coherence window of 3×3 pixels as described by,

$$\text{COH} = \frac{|\sum_i s_{1,i} s_{2,i}^*|}{\sqrt{\sum_i |s_{1,i}|^2 \sum_i |s_{2,i}|^2}}$$

where subscript i denotes pixel i . In order to compensate for the antenna gain loss at the scene sides due to the decreasing signal-to-noise ratio (SNR), a correction based on the noise floor polynomial (available in the TanDEM-X meta data) was applied, as previously described (Chen et al. 2016; Kugler et al. 2014; Persson et al. 2017).

The local incidence angle (INC) was computed based on the satellite system geometry and the ALS DTM. An initial estimate of the system geometry is based on the state vectors (TanDEM-X meta data), and it was then improved with a cross-correlation procedure between the multi-looked intensity images and the ALS DTM which was converted to range-doppler coordinates (RDC) and used to simulate the assumed intensity response, based on the satellite configuration.

In summary, five InSAR observables were generated and used as base metrics. These included PH and its standard deviation PH SD, INC, COH, and S_0 .

ALS base metrics

TerraSolid (Terrasolid Oy, Espoo, Finland) was used for initial data processing and ground classification of the ALS data. Subsequent processing was carried out in the LAsTools software (RapidLasso, Gilching, Germany) and included noise removal, height normalisation, and generation of widely used forest inventory predictive metrics describing the height distribution of returns (e.g. percentile, skew, kurtosis, standard deviation, and modal heights) along with metrics capturing information on the vertical forest structure that are often described as the key advantage of ALS (e.g. vertical complexity index or VCI, canopy cover and canopy density). A detailed description of the processing of the ALS base metrics is given in Pearse et al. (2018).

Canopy height models

Two types of CHM raster datasets were derived for the InSAR predictors. The Radar CHM was constructed by subtracting the WorldDEM™ DTM from the Radar DSM. The Mixed CHM was computed as the difference between the ALS DTM bilinearly resampled to 10.7 m and the WorldDEM™ DSM (Fig. 2). Both of the two CHM products had a ground resolution of 10.7 m and average height, within each plot from both CHMs, was used as the predictor from the CHM. Erroneous values less than zero were discarded. Raster processing was undertaken using the arcpy module in Python 3.6.

For the ALS counterpart, a CHM raster that was free of data pits caused by deep laser penetration into tree crowns was derived by implementing the algorithm of Khosravipour et al. (2014). Standard CHM metrics (e.g. average, maximum, minimum, median, standard deviation) and heights of different quantiles were extracted from each plot and used within the modelling.

Textural metrics

The textural attributes of canopy surface models have previously been shown to be related to forest biophysical variables in this forest type (Pearse et al. 2018). To capture these attributes, textural metrics based on the grey-level co-occurrence matrix (GLCM) statistics were derived using a 3×3 -pixel windows size applied to each of three CHM datasets (Radar CHM, Mixed CHM, and ALS CHM) at directions of 0° , 45° , 90° , and 153° . These textural predictors included *contrast*, *correlation*, *dissimilarity*, *entropy*, *homogeneity*, *mean*, *second moment*, and *variance*. GLCM was implemented using the *gldm* package (Zvoleff 2019) in R statistical software 3.5.3 (R. Core Team 2019).

Data analysis

All the InSAR and ALS predictors, in raster format, described above, were reprojected to the national coordinate system (NZTM2000) and heights to a consistent reference ellipsoid (GRS80). Mean values per metric were extracted per plot using a circular feature with a radius of 14 m with the centre defined by the field GPS coordinates. This process was executed using the zonal statistics using ArcGIS 10.6 (ESRI, Redlands CA, USA).

Relationships between Radar and ALS surfaces

Visual comparisons were made between the DTM and CHMs extracted from InSAR and ALS. Using ALS surfaces as the observed reference, plot level values of DTM, CHM, and DSM, were regressed against their InSAR counterparts (both based on the WorldDEM and the InSAR base metrics). Residuals from these relationships were plotted against ALS slope estimates produced using the DEM analysis tools from the Geospatial Data Abstraction Library (GDAL) 2.2.4 (GDAL/OGR contributors 2019). The ALS DTM was bilinearly resampled to 10.7 m before being used to compute the slope values using a 3 x 3-pixel neighbourhood.

The errors between the reference and InSAR products were characterised using all data, and data categorised within four slope classes, using root mean square error (RMSE), the coefficient of determination (R^2), and the mean bias error (MBE), which were calculated, respectively, as,

$$RMSE = \sqrt{\frac{\sum_{i=1}^n (\hat{y}_i - y_i)^2}{n}}$$

$$R^2 = \frac{\sum_i (\hat{y}_i - \bar{y})^2}{\sum_i (y_i - \bar{y})^2}$$

$$MBE = \frac{1}{n} \sum_{i=1}^n y_i - \hat{y}_i$$

where y_i is the observed value, \hat{y}_i is the predicted value in plot i , \bar{y} is the average of the observed values, and n is the number of plots.

Prediction of Forest Inventory Variables

The precision of bivariate correlations among the four biophysical variables and all metrics derived from the InSAR and ALS datasets were examined to gain insight into the predictors within each of the two datasets that were most strongly related to H , G , N , and TSV .

The random forest (RF) regression approach was then used to estimate the four biophysical variables of interest. Predictive variables that were used in the modelling are given in Appendices 1 and 2. Separate models were created using InSAR and ALS data and precision of these models were compared. The five created InSAR models included variables from the following groups (i) base metrics, (ii) base metrics and the Radar CHM, (iii) base metrics and the Mixed CHM, (iv) base metrics and the Radar CHM and texture metrics, (v) base metrics and the Mixed CHM and texture metrics. The ALS models included metrics that were selected from the following three groups (i) base metrics, (ii) base metrics and CHM metrics and (iii) base metrics, CHM metrics and textural metrics.

There is an increasing interest in using RF to predict forest inventory attributes (Karila et al. 2015). RF adds a random element to bootstrap aggregation or bagging in the sense that each node of the regression trees is split using the best randomly chosen predictor. It is also known to be robust to overfitting though hyper-parameters that can be tuned to prevent this occurring. The RF approach draws random regression trees with replacement from two-thirds of the data and retains one-third for testing. The samples that are left out become the out-of-bag samples and act as the

test set. While this removes the need to set aside a test set, it is empirically proven to be as accurate as using a test set with the same size as the training set (Breiman 2001).

RF model fitting and accuracy assessment were implemented using the machine learning module scikit-learn 0.20.3 (Pedregosa et al. 2011) in Python 3.6. In this study, three hyper-parameters were selected using a 10-cross fold grid search for each model. These were: the number of decision trees in the forest (from 200 to 1000 by increments of 50), minimum number of samples required to split an internal node (3, 4, 5), and the minimum number of samples at a leaf node (3, 4, 5). For each biophysical variable, each predictor was randomly permuted one at a time then RF was applied to the dataset to determine which features result in the highest gain in information based on R^2 . Predictors with a greater impact on R^2 were considered to be the most important features. Each model was run 100 times to take the randomness into account. The mean out-of-bag samples for all the runs were used to test the accuracy of the model through R^2 , RMSE and the percent RMSE% that was calculated from $RMSE\% = 100 (RMSE/\bar{y})$, where \bar{y} is the average of the observed values.

Results

Data range

Wide variation was noted between all stand biophysical variables (Table 2). Variation in the earlier acquired Radar dataset was broad, with variation in H , G , N , and TSV ranging, respectively four-fold, 25-fold, 13-fold and 37-fold. Similar variation was noted for the later acquired ALS with variation in H , G , N , and TSV , ranging, respectively, three-fold, 15-fold, 12-fold and 22-fold. Between the Radar and ALS acquisition there were small increases in H , G and TSV with these variables increasing, respectively, on average by 6.92, 8.74 and 13.3%. In contrast, N declined by 1.49% over the period between these acquisitions as the growth model simulated tree mortality (Table 2).

Table 2. Summary statistics for inventory plot data. Shown are the mean, standard deviation (SD) and the range from 171 plots.

| Variable | Mean | SD | Range |
|-------------------------------------|------|------|-------------|
| Radar | | | |
| Mean top height (m) | 29.6 | 5.07 | 10.8 – 39.4 |
| Basal area ($m^2 ha^{-1}$) | 49.1 | 18.1 | 3.41 – 86.6 |
| Stand density (stems ha^{-1}) | 340 | 153 | 66.7 – 842 |
| Total stem volume ($m^3 ha^{-1}$) | 469 | 188 | 23.9 – 894 |
| ALS | | | |
| Mean top height (m) | 31.8 | 4.88 | 13.2 – 41.2 |
| Basal area ($m^2 ha^{-1}$) | 53.8 | 17.4 | 5.71 – 88.5 |
| Stand density (stems ha^{-1}) | 335 | 149 | 66.7 – 815 |
| Total stem volume ($m^3 ha^{-1}$) | 541 | 193 | 45.1 – 974 |

Similarly, wide variation was noted in the predictive metrics used within the InSAR (Appendix 1) and ALS datasets (Appendix 2). Variation within metrics for the InSAR metrics was wide, averaging 14-fold across the 24 generated variables, with mean variation ranging from 13-fold for the base metrics, to 16-fold for the CHM metrics to 11-fold and 18-fold for the textural metrics derived, respectively, from the Mixed and Radar CHM. The variables that showed the greatest variation were the textural metrics *variance* (61-fold range) and *contrast* (49-fold range) for the Radar CHM and the textural metric *variance* for the Mixed CHM (39-fold range).

The 45 metrics extracted from the ALS ranged by an average of 17-fold, with metric variation ranging between the three metric classes from eight-fold for the textural metrics to 16-fold for the base metrics to 28-fold for the metrics extracted from the CHM. The metrics demonstrating the most variation were: CHM p25 (225-fold range), p25 (125-fold range) and b10 (124-fold range).

Relationships between the ALS and Radar DTM, DSM and CHM

Across the area of interest, the Radar DTM and DSM were both highly correlated to their ALS counterparts, with respective R^2 's of 0.998 and 0.999 (Fig. 3a, b). These high correlations and the apparent visual similarity in these surfaces (Fig. 4) predominantly reflected the wide range in elevation (148 to 812 m) covered by these surfaces which inflates values for the R^2 and masks subtle fine-scale changes in elevation. In contrast the RMSE, which is more reflective of the utility of these surfaces, showed only a moderate degree of precision (Table 3), with mean values of, respectively, 8.09 m and 4.58 m for the Radar DTM and DSM. The RMSE for both surfaces was sensitive to slope with values increasing two to three-fold between slopes of 10 – 20° to slopes of 40 – 50° for which values for the DTM and DSM were, respectively, 10.17 and 6.02 m (Table 3).

The DTM and DSM surfaces derived from the radar were biased. Overall, the reference ALS DTM and DSM were, respectively, on average 5.93 and 0.92 m lower than those of the corresponding Radar surfaces (Table 3; Figs. 3e, f). The degree of this bias increased markedly with slope (Table 3). The difference between the ALS and Radar DTM ranged from a mean of -0.09 m for slopes of 10–20° to -9.44 m for slopes of 40–50, while the differences between the ALS and Radar DSM ranged from 0.08 m for slopes of 20–30° to -4.33m for slopes of 40–50° (Table 3; Figs. 3e, f).

The ALS CHM was only weakly related to the CHM derived from the Radar (Fig. 3d) base layers ($R^2 = 0.14$; RMSE = 11.1 m). The mean RMSE of 11.1 m reflected the poor precision of this relationship and the RMSE showed some increase between slopes of 10 – 20° but stabilised after this point (Table 3). The relationship between these surfaces was very biased with values for the ALS CHM exceeding those of the Radar by an average of 10.1 m. This mean bias error was sensitive to slope and increased to 20° after which point it stabilised (Table 3; Fig. 3h).

The Mixed CHM, derived from the Radar DSM and ALS DTM, was more strongly correlated to the ALS CHM but the correlation was only of a moderate strength with R^2 of 0.49 (Fig. 3c). The mean RMSE was 5.95 m and values for RMSE were relatively unaffected by slope (Table 3). This surface was biased and values for the ALS CHM exceeded those of the Mixed CHM by a mean of 4.09 m, with values for this bias declining as slope increased (Table 3; Fig. 3g).

Maps of the three CHMs clearly show the restricted height range in the surfaces derived from Radar (Fig. 5). Although height from the Radar surface broadly corresponded to features evident in the ALS CHM, the height range was considerably reduced (max. heights of 37.6 m vs. 45.0 m). The Mixed CHM did demonstrate a wider height range, more closely aligned to that of the ALS CHM (max. heights of 45.1 m vs. 45.0 m), and closer correspondence in height changes were evident throughout the forest.

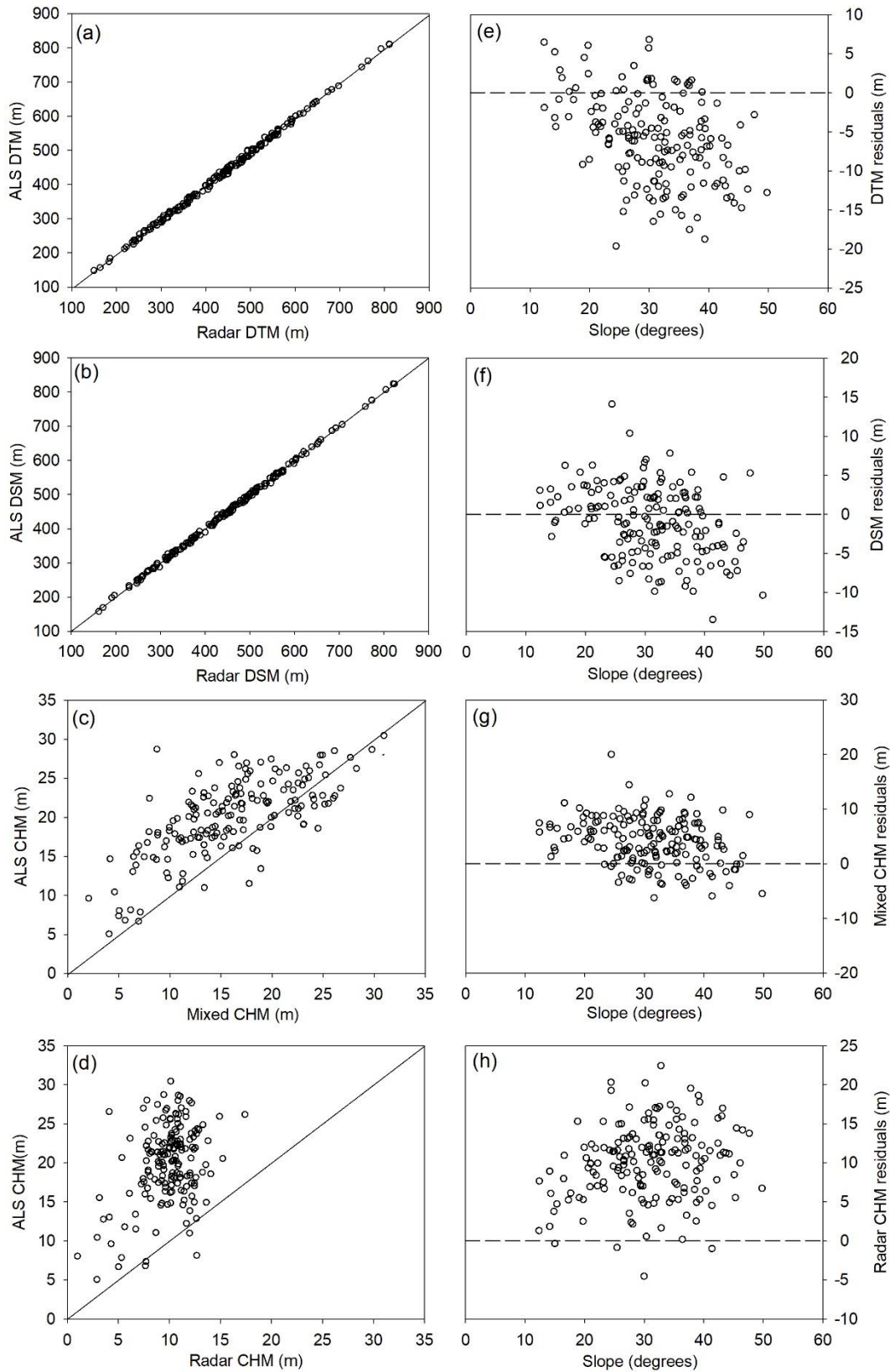


Figure 3. Relationship between the Radar (a) DTM, (b) DSM, (c) Mixed CHM, (d) Radar CHM with their corresponding ALS counterparts. Shown on the right-hand side are residual values from these four relationships plotted against slope derived from the ALS DTM.

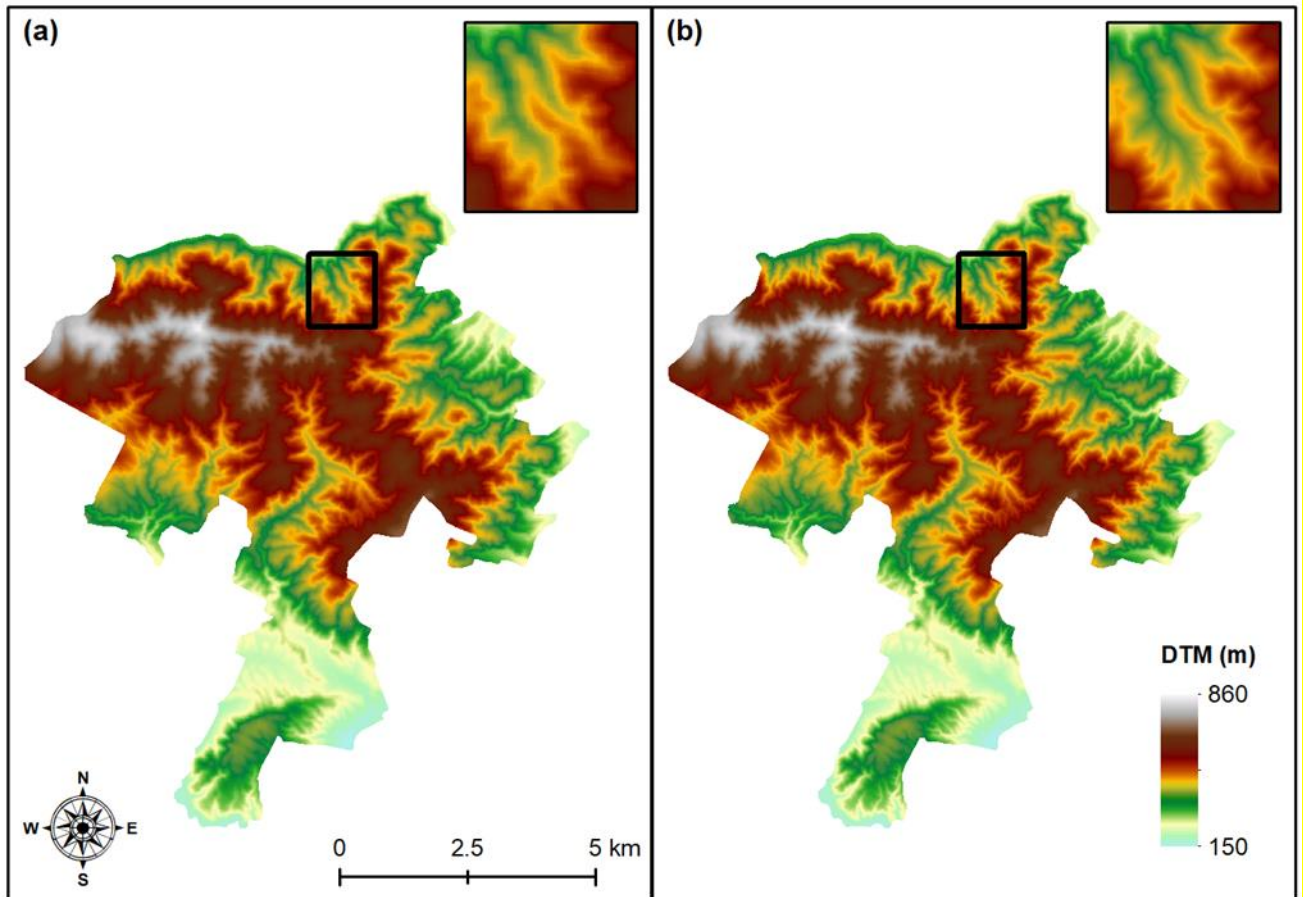


Figure 4. Comparison of (a) 10.7 m resolution Radar DTM sourced from the WorldDEM with a (b) 1.0 m DTM captured by ALS. The inset map highlights the differences between the two DTMs at a finer scale.

Table 3. Summary statistics showing the influence of slope on root mean square error (RMSE) and mean bias error (MBE) for the four surfaces derived from radar data (Radar DTM, Radar DSM, Radar CHM and Mixed CHM). For each of the four radar surfaces the errors were determined using the corresponding ALS surface as a reference. The number of plots within each of the four slope classes was 17 (10–20°), 59 (20–30°), 74 (30–40°) and 21 (40–50°). The RMSE and MBE is also shown for all plots.

| Statistic | Slope | | | | All plots |
|------------------|--------|--------|--------|--------|-----------|
| | 10–20° | 20–30° | 30–40° | 40–50° | |
| Radar DTM | | | | | |
| RMSE (m) | 4.51 | 6.81 | 8.95 | 10.17 | 8.09 |
| MBE (m) | -0.09 | -4.69 | -7.27 | -9.44 | -5.93 |
| Radar DSM | | | | | |
| RMSE (m) | 2.96 | 4.57 | 4.41 | 6.02 | 4.58 |
| MBE (m) | 1.74 | 0.08 | -1.37 | -4.33 | -0.92 |
| Radar CHM | | | | | |
| RMSE (m) | 7.31 | 10.59 | 12.15 | 11.27 | 11.11 |
| MBE (m) | 6.17 | 9.71 | 11.18 | 10.43 | 10.08 |
| Mixed CHM | | | | | |
| RMSE (m) | 6.58 | 6.58 | 5.70 | 4.12 | 5.95 |
| MBE (m) | 6.07 | 4.88 | 3.90 | 0.95 | 4.09 |

Correlations between biophysical variables and metrics derived from ALS and Radar

Bivariate relationships between the four biophysical variables and metrics were generally stronger for variables derived from ALS than those derived from Radar (Table 4). When averaged over each biophysical variable the mean R for these bivariate relationships ranged from three-fold to five-fold higher for ALS than those for Radar, with the largest absolute differences evident for H (mean $R = 0.59$ vs. 0.23), and TSV (mean $R = 0.58$ vs. 0.25) but substantial differences were also evident for G (mean $R = 0.47$ vs. 0.25) and N (mean $R = 0.25$ vs. 0.16). Similarly, the maximum correlation for each biophysical variable was also markedly higher for metrics derived from ALS than those derived from Radar (Table 4), with the smallest absolute differences occurring for H (max. $R = 0.95$ vs. 0.73) and TSV (max. $R = 0.83$ vs. 0.59) with larger differences occurring for G (max. $R = 0.76$ vs. 0.46) and N (max. $R = 0.63$ vs. 0.29).

Using metrics derived from ALS, H was most closely correlated with the upper percentiles (90th to 99.5th), derived from either the point cloud or the CHM (Table 4). These five predictors were strongly and positively related to H (R range of $0.92 - 0.95$). Basal area was most strongly predicted by positive relationships with the two canopy cover metrics, CCov 10 m and CCov 5 m, which had, respectively, R values of 0.76 and 0.72 . The standard deviation of the canopy height model was most closely correlated with N and this relationship had an R of -0.63 . The mean height derived from the point cloud and CHM and the two textural metrics, *mean* and *variance*, were most strongly related to TSV . All of these four bivariate relationships were positive and had R ranging from $0.81 - 0.83$ (Table 4).

Using metrics derived from the Radar data, the mean height from the Mixed CHM and the textural metrics *mean* and *variance*, derived from this CHM, were most strongly related to H (Table 4). These relationships were all positive and had R ranging from $0.70 - 0.73$. Similarly, these three variables were also most strongly related to TSV and the correlation coefficients of the positive relationships between these variables and TSV ranged from $0.55 - 0.59$. In contrast, the Radar CHM, the associated textural metric *mean*, and the S_0 were the variables most strongly related to both G and N . The R for the three most important predictors of G ranged from $0.43-0.46$, while the three strongest predictors of N had R ranging from $0.26 - 0.29$ (Table 4).

Models of biophysical variables

Models using ALS data

The range in precision of random forest models created from ALS varied widely between biophysical variables (Table 5). The most precise models created for H , G , N , and TSV had respective RMSE values of 1.80 m, 11.6 m² ha⁻¹, 108 stems ha⁻¹, 105 m³ ha⁻¹, RMSE% of respectively 5.67 , 21.5 , 32.3 , and 19.4% , with respective R^2 of 0.86 , 0.56 , 0.47 and 0.70 . Among the four biophysical variables, the most precise model for N was created using all the available metrics while the most precise models of H and TSV used only the base and CHM metrics and the model of G used only the base metrics (Table 5). Gains in precision achieved using all metrics over the base metrics were minor as evidenced by respective changes in the RMSE% between these two groups of -0.25 , 0.09 , -1.04 and -0.10% for H , G , N , and TSV . Measured values for the final models showed little apparent bias when plotted against predicted values (Fig. 6). The residual values from these models also showed little apparent bias when plotted against slope (Fig. 7).

The key metrics within the most precise of the four ALS models are given in Table 5. For H , the key metrics predominantly describe the upper canopy percentiles (p90 – p99.5) of the CHM. The model of TSV was most sensitive to mean height from either the point cloud or CHM and b10. The most important metrics for G were predominantly canopy cover or the ALS metrics from within the lower canopy (i.e. b10). The model of N was most strongly influenced by the standard deviation of the CHM and canopy cover metrics (Table 5).

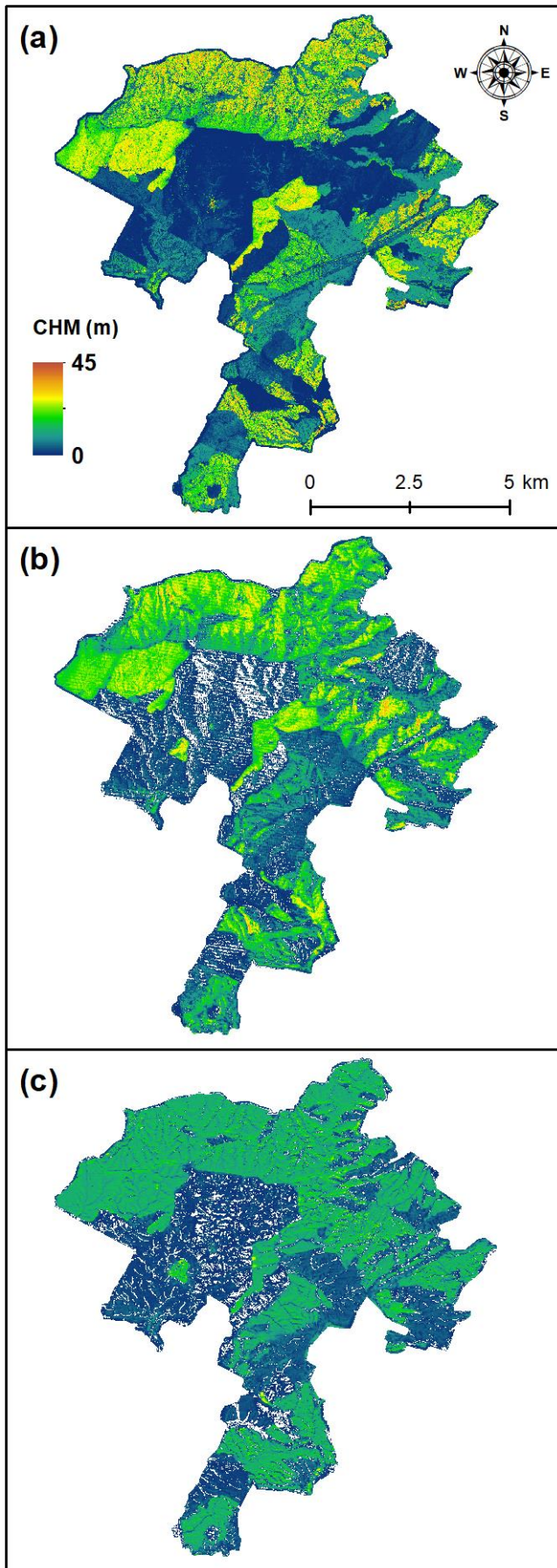


Figure 5. Maps of the (a) ALS CHM, (b) mixed CHM derived using the ALS DTM and radar DSM, and (c) Radar CHM derived using the Radar DTM and DSM.

Table 4. The predictive precision of simple bivariate relationships between Mean Top Height (H), Basal Area (G), Stand Density (N) and Total Stem Volume (TSV) and metrics derived from ALS (left columns) and Radar (right columns). Predictive precision is given between the correlation coefficient (R) which has been categorised by grayscale into either positive or negative relationships of very high ($R = 0.800 - 1.000$), high ($R = 0.600 - 0.799$), moderate ($R = 0.400 - 0.599$), weak ($R = 0.200 - 0.399$) and very weak ($R < 0.200$) strength. For each biophysical variable the underlined bolded values show the metrics with the highest R . The full name of each variable is given in Appendices 1 and 2.

| Predictor | Predictions using ALS data | | | | Predictor | Predictions using Radar data | | | |
|----------------------------|----------------------------|-------|-------|-------|---------------------------------------|------------------------------|-------|-------|-------|
| | H | G | N | TSV | | H | G | N | TSV |
| Base Metrics | | | | | Base Metrics | | | | |
| Max Height | 0.92 | 0.30 | -0.38 | 0.57 | PH | 0.46 | 0.04 | -0.18 | 0.17 |
| Mean Height | 0.76 | 0.64 | 0.08 | 0.82 | PH SD | 0.00 | 0.12 | 0.05 | 0.10 |
| Quadratic M | 0.84 | 0.59 | -0.03 | 0.79 | COH | -0.27 | 0.07 | 0.09 | -0.03 |
| SD | 0.88 | 0.24 | -0.40 | 0.50 | INC | -0.08 | 0.15 | 0.09 | 0.17 |
| Skew | -0.33 | -0.69 | -0.44 | -0.69 | S_0 | -0.19 | -0.43 | -0.26 | -0.42 |
| Kurtosis | -0.22 | -0.23 | 0.00 | -0.19 | Canopy Height Model | | | | |
| CV | -0.28 | -0.69 | -0.45 | -0.66 | Mixed CHM | 0.70 | 0.41 | -0.12 | 0.59 |
| Mode | 0.53 | 0.61 | 0.11 | 0.71 | Radar CHM | 0.11 | 0.43 | 0.29 | 0.36 |
| p99.5 | 0.95 | 0.32 | -0.37 | 0.60 | Texture derived from Mixed CHM | | | | |
| p99 | 0.95 | 0.33 | -0.35 | 0.61 | Contrast | 0.16 | -0.27 | -0.15 | -0.17 |
| p95 | 0.94 | 0.40 | -0.29 | 0.66 | Correlation | -0.03 | 0.05 | 0.03 | 0.05 |
| p90 | 0.92 | 0.46 | -0.22 | 0.71 | Dissimilarity | 0.17 | -0.28 | -0.17 | -0.19 |
| p75 | 0.81 | 0.57 | -0.04 | 0.76 | Entropy | 0.22 | -0.20 | -0.23 | -0.10 |
| p50 | 0.68 | 0.65 | 0.15 | 0.79 | Homogeneity | -0.18 | 0.26 | 0.18 | 0.18 |
| p25 | 0.40 | 0.63 | 0.32 | 0.71 | Mean | 0.73 | 0.39 | -0.15 | 0.59 |
| b99 | -0.02 | 0.20 | 0.26 | 0.12 | Sec. moment | -0.22 | 0.20 | 0.24 | 0.09 |
| b95 | -0.20 | -0.16 | -0.03 | -0.25 | Variance | 0.71 | 0.34 | -0.17 | 0.55 |
| b90 | -0.26 | -0.24 | -0.06 | -0.33 | Texture derived from Radar CHM | | | | |
| b80 | -0.29 | -0.37 | -0.16 | -0.44 | Contrast | 0.10 | -0.23 | -0.09 | -0.17 |
| b75 | -0.31 | -0.42 | -0.20 | -0.49 | Correlation | -0.23 | -0.34 | -0.17 | -0.35 |
| b50 | -0.35 | -0.58 | -0.33 | -0.63 | Dissimilarity | 0.11 | -0.24 | -0.13 | -0.17 |
| b25 | -0.37 | -0.66 | -0.33 | -0.67 | Entropy | 0.13 | -0.21 | -0.18 | -0.12 |
| b10 | -0.35 | -0.66 | -0.27 | -0.65 | Homogeneity | -0.12 | 0.20 | 0.15 | 0.13 |
| CCov DBH | 0.11 | 0.41 | 0.40 | 0.36 | Mean | 0.16 | 0.46 | 0.28 | 0.41 |
| CCov 5m | 0.36 | 0.72 | 0.42 | 0.69 | Sec. moment | 0.01 | 0.05 | -0.12 | 0.22 |
| CCov 10m | 0.47 | 0.76 | 0.38 | 0.78 | Variance | 0.11 | 0.39 | 0.24 | 0.34 |
| VCI | 0.75 | 0.57 | -0.01 | 0.68 | Key R range | | | | |
| Canopy Height Model | | | | | 0.800 – 1.000; -1.000 – -0.800 | | | | |
| CHM Max | 0.93 | 0.30 | -0.39 | 0.57 | 0.600 – 0.799; -0.799 – -0.600 | | | | |
| CHM Mean | 0.72 | 0.68 | 0.16 | 0.83 | 0.400 – 0.599; -0.599 – -0.400 | | | | |
| CHM Median | 0.68 | 0.65 | 0.17 | 0.78 | 0.200 – 0.399; -0.399 – -0.200 | | | | |
| CHM SD | 0.47 | -0.29 | -0.63 | -0.10 | 0 – 0.199; -0.199 – 0 | | | | |
| CHM p99 | 0.95 | 0.32 | -0.36 | 0.60 | | | | | |
| CHM p95 | 0.95 | 0.37 | -0.31 | 0.65 | | | | | |
| CHM p90 | 0.94 | 0.43 | -0.25 | 0.69 | | | | | |
| CHM p75 | 0.83 | 0.57 | -0.04 | 0.76 | | | | | |
| CHM p50 | 0.68 | 0.65 | 0.17 | 0.78 | | | | | |
| CHM p25 | 0.49 | 0.68 | 0.33 | 0.77 | | | | | |
| Texture | | | | | | | | | |
| Contrast | 0.63 | -0.04 | -0.48 | 0.18 | | | | | |
| Correlation | 0.33 | -0.02 | -0.44 | 0.04 | | | | | |
| Dissimilarity | 0.67 | 0.14 | -0.37 | 0.32 | | | | | |
| Entropy | 0.51 | 0.57 | 0.18 | 0.61 | | | | | |
| Homogeneity | -0.63 | -0.43 | 0.08 | -0.54 | | | | | |
| Mean | 0.72 | 0.68 | 0.16 | 0.83 | | | | | |
| Sec. moment | -0.44 | -0.56 | -0.25 | -0.59 | | | | | |
| Variance | 0.80 | 0.60 | 0.03 | 0.81 | | | | | |

Table 5. Variation in the precision of models of biophysical variables created using either InSAR or ALS data and using different combinations of the available metrics. Statistics describing precision include the coefficient of determination (R^2) and root mean square error (RMSE) expressed as value and as a percentage of the mean (RMSE%) for each biophysical variable. The top three most important features for each model are also shown. For each biophysical variable the underlined bolded values show the best performing models.

| ALS | | | | |
|---|--------------------|--------------------|--------------------|--|
| Biophysical Variable | RMSE | RMSE% | R^2 | Most important variables |
| Base Metrics | | | | |
| Mean top height (m) | 1.88 | 5.92 | 0.85 | p99, p95, p99.5 |
| Basal area ($m^2 ha^{-1}$) | <u>11.6</u> | <u>21.5</u> | <u>0.56</u> | <u>CCov 5m, CCov 10m, b10</u> |
| Stand density (stems ha^{-1}) | 112 | 33.3 | 0.43 | CCov 5m, CV, Max Height |
| Total stem volume ($m^3 ha^{-1}$) | 106 | 19.5 | 0.70 | Mean Height, CCov 10m, CCov 5m |
| Base Metrics + CHM | | | | |
| Mean top height (m) | <u>1.80</u> | <u>5.67</u> | <u>0.86</u> | <u>CHM p90, CHM p95, p99</u> |
| Basal area ($m^2 ha^{-1}$) | 11.7 | 21.7 | 0.55 | CCov 5m, b10, CCov 10m |
| Stand density (stems ha^{-1}) | 109 | 32.4 | 0.46 | CHM SD, Max Height, b25 |
| Total stem volume ($m^3 ha^{-1}$) | <u>105</u> | <u>19.4</u> | <u>0.70</u> | <u>CHM Mean, b10, Mean Height</u> |
| Base Metrics + CHM + Texture | | | | |
| Mean top height (m) | 1.80 | 5.67 | 0.86 | CHM p90, CHM p95, CHM p99 |
| Basal area ($m^2 ha^{-1}$) | 11.6 | 21.6 | 0.56 | CCov 5m, CCov 10m, b10 |
| Stand density (stems ha^{-1}) | <u>108</u> | <u>32.3</u> | <u>0.47</u> | <u>CHM SD, CCov 10m, CCov 5m</u> |
| Total stem volume ($m^3 ha^{-1}$) | 105 | 19.4 | 0.70 | CHM Mean, b10, Mean Height |
| InSAR | | | | |
| Biophysical Variable | RMSE | RMSE% | R^2 | Most important variables |
| Base Metrics | | | | |
| Mean top height (m) | 4.21 | 14.2 | 0.31 | PH, COH, INC |
| Basal area ($m^2 ha^{-1}$) | 16.8 | 34.2 | 0.16 | So, PH SD, PH |
| Stand density (stems ha^{-1}) | 157 | 46.0 | 0.02 | So, PH SD, PH |
| Total stem volume ($m^3 ha^{-1}$) | 169 | 36.1 | 0.19 | So, PH SD, PH |
| Base Metrics + Radar CHM | | | | |
| Mean top height (m) | 4.23 | 14.3 | 0.30 | PH, COH, INC |
| Basal area ($m^2 ha^{-1}$) | 15.8 | 32.2 | 0.24 | Radar CHM, So, PH SD |
| Stand density (stems ha^{-1}) | 149 | 43.7 | 0.08 | Radar CHM, So, PH SD |
| Total stem volume ($m^3 ha^{-1}$) | 166 | 35.4 | 0.22 | So, INC, Radar CHM |
| Base Metrics + Mixed CHM | | | | |
| Mean top height (m) | 3.27 | 11.1 | 0.58 | Mixed CHM, INC, COH |
| Basal area ($m^2 ha^{-1}$) | 15.1 | 30.7 | 0.31 | Mixed CHM, So, COH |
| Stand density (stems ha^{-1}) | 154 | 45.2 | 0.03 | So, Mixed CHM, PH SD |
| Total stem volume ($m^3 ha^{-1}$) | 144 | 30.8 | 0.41 | Mixed CHM, So, PH SD |
| Base Metrics + Radar CHM + Texture | | | | |
| Mean top height (m) | 4.25 | 14.4 | 0.29 | PH, COH, INC |
| Basal area ($m^2 ha^{-1}$) | 15.4 | 31.4 | 0.28 | Radar CHM, So, PH SD |
| Stand density (stems ha^{-1}) | <u>147</u> | <u>43.2</u> | <u>0.09</u> | <u>Radar CHM, PH, So</u> |
| Total stem volume ($m^3 ha^{-1}$) | 164 | 34.9 | 0.24 | So, PH SD, INC |
| Base Metrics + Mixed CHM + Texture | | | | |
| Mean top height (m) | <u>3.18</u> | <u>10.8</u> | <u>0.60</u> | <u>Mean, Variance, INC</u> |
| Basal area ($m^2 ha^{-1}$) | <u>14.9</u> | <u>30.4</u> | <u>0.32</u> | <u>So, Mixed CHM, COH</u> |
| Stand density (stems ha^{-1}) | 153 | 44.9 | 0.03 | So, PH SD, PH |
| Total stem volume ($m^3 ha^{-1}$) | <u>144</u> | <u>30.7</u> | <u>0.41</u> | <u>Mean, So, Mixed CHM</u> |

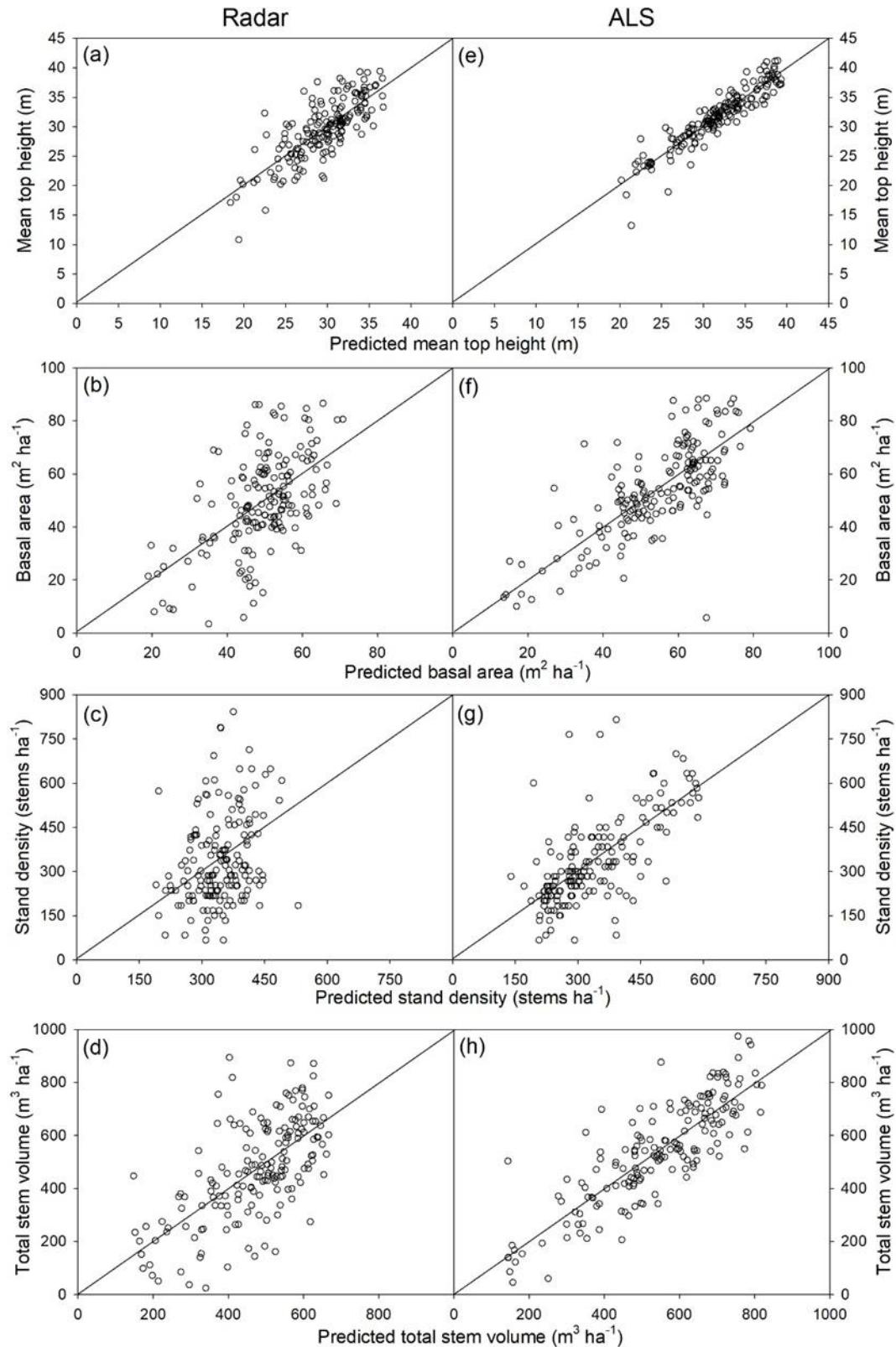


Figure 6. The relationship between predicted and observed values for biophysical variables predicted using metrics extracted from Radar (left panels – a, b, c, d) and ALS (right panels, e, f, g, h). Shown within the figure are relationships for mean top height (a, e), basal area (b, f), stand density (c, g) and total stem volume (d, h). The 1: 1 line is shown on each panel as a diagonal dashed line.

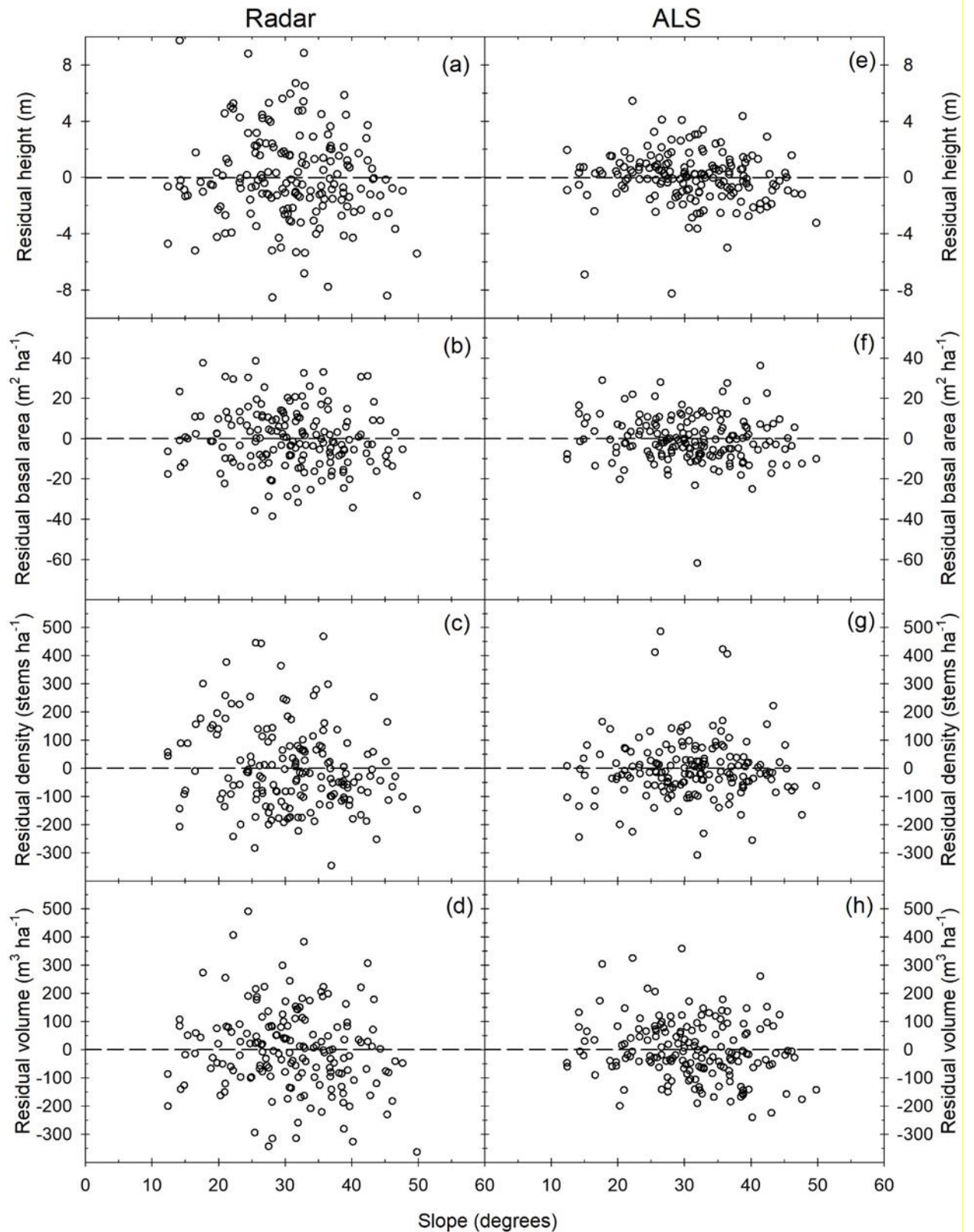


Figure 7. The relationship between slope and residual values (observed – predicted) extracted from the final models that use metrics obtained from Radar (left panels – a, b, c, d) and ALS (right panels, e, f, g, h) using the Random Forest approach. Shown within the figure are relationships for residuals extracted from models of mean top height (a, d), basal area (b, f), stand density (c, g) and total stem volume (d, h). The dashed horizontal line is shown for reference at $y = 0$.

Models using InSAR data

Compared to the use of ALS, predictions of the four biophysical variables using metrics derived from InSAR were considerably less precise (Table 5). The most precise models created for *H*, *G*, *N*, and *TSV* had respective RMSE of 3.18 m, 14.9 m² ha⁻¹, 147 stems ha⁻¹, 144 m³ ha⁻¹, with respective *R*² of 0.60, 0.32, 0.09, and 0.41. These models had respective RMSE% of 10.8, 30.4, 43.2, and 30.7% and these values were respectively, 5.13, 8.90, 10.9, and 11.3% higher than RMSE% values obtained from ALS models. (Table 5). Plots of predictions against measured values for the final models showed more bias than the corresponding plots using models derived from ALS metrics (Fig. 6). The extent of this bias was most marked for *G*, *N*, and *TSV*, with overprediction occurring at low measured values and underprediction occurring at high values for each of these three biophysical variables (Fig. 6). However, there was little apparent bias when residual values for each of the four models were plotted against slope (Fig. 7).

The extent of gains noted in the RF models as a larger number of predictors were added ranged widely between the four biophysical variables (Fig. 8). The most precise models for *H*, *G*, and *TSV* used all of the metrics. Addition of metrics from the Mixed CHM resulted in respective reductions in RMSE% of 3.1, 3.5, and 5.3% for models of *H*, *G*, and *TSV* with addition of textural metrics providing further reductions for *H* and *G* models of 0.3% for both variables (Fig. 8). The most precise model of *N* included base metrics and metrics from the Radar CHM. Addition of metrics from the Radar CHM reduced the RMSE% of the base model for *N* by 2.3% with addition of textural metrics reducing the RMSE% further by 0.5% (Fig. 8).

The key metrics within the model of *H* included the textural metrics *mean* and *variance*, and the local incidence angle from the base Radar metrics (Table 5). Radar backscatter (*S*₀) was the strongest predictor for *G*, followed by Mixed CHM and COH, while it was also included in the most important predictors for *N* along with Radar CHM and the standard deviation for PH. The key metrics for the model of *TSV* included the textural metric *mean*, *S*₀ and mean height from the mixed CHM (Table 5).

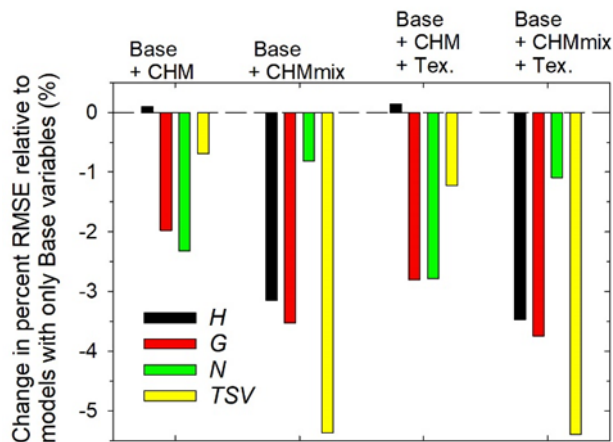


Figure 8. Changes in the percentage RMSE (RMSE%), relative to models that include only base variables, for the four groups of metrics that include various combinations of the Radar CHM (CHM), Mixed CHM (CHMmix) and Textural metrics (Tex.). The four biophysical variables, mean top height (*H*), basal area (*G*), stand density (*N*) and total stem volume (*TSV*) are denoted by, respectively, black, red, green and yellow columns.

Discussion

In this study, we compared the utility of InSAR with ALS-derived metrics to predict the forest inventory variables *H*, *G*, *N*, and *TSV* for a temperate plantation forest with steep and variable terrain. Overall, the ALS models were more precise and less biased than the InSAR models in prediction of the four biophysical variables. Although InSAR models were clearly less precise than ALS models, the precision was consistent with previous studies and these models did provide a reasonable level of precision for *H* and *TSV*, which was significantly improved through inclusion of

metrics from the Mixed CHM. Despite the sensitivity of the InSAR derived surfaces to topography, prediction errors from the final InSAR models of biophysical variables were found to be insensitive to variation in stand slope.

The precision of models developed from ALS were broadly consistent with those that have been previously developed. The RMSE% of the best *H* model (5.67 %) was comparable to the results of earlier studies which ranged from 3.0–9.6% (Holmgren 2004; Persson and Fransson 2017; Stone et al. 2011; Yu et al. 2015) while the precision of the best model of *TSV* (19.4 %) was within the reported range of 11–20% found in previous studies (Holmgren 2004; Rahlf et al. 2014; Yu et al. 2015). Our model of *G* had a slightly lower precision (RMSE% = 21.5%), than many other reported studies where RMSE% ranged between 10–17% (Holmgren 2004; Yu et al. 2015) but was comparable to a study by Shang et al. (2019) which had an RMSE of 20%. The least precise ALS model among the four forest biophysical variables was stand density (RMSE% = 32.3%) which was markedly less precise than previous stand density models where RMSE% ranged from 23.4 – 25.0% (Shang et al. 2019; Stone et al. 2011).

Though the InSAR models had markedly lower precision than the ALS models the precision of the best models were generally consistent with those that have been previously developed. The InSAR model for *H* (RMSE% = 10.8%) was at the upper end of the precision range reported by Karila et al. (2015) which had RMSE% of 20.0–25.2% and Persson and Fransson (2017) where RMSE% ranged from 9–16%. These studies were based on measurements from plots with respective areas of 300 and 315 m². In contrast, the *H* model of Yu et al. (2015), which used plots with an area of 1 024 m², had a slightly superior RMSE% of 9.53%. The best *TSV* model in this study (RMSE% = 30.7%) was found to be more precise than most studies which had an RMSE% ranging from 32.2 – 44% (Karila et al. 2015; Rahlf et al. 2014; Solberg et al. 2013) but was less precise than the model developed by Yu et al. (2015) which had RMSE% of 21.0%. Very little research has developed models of *N* and *G* based on InSAR metrics. However, Solberg et al. (2017) noted a positive weak correlation between *N* and InSAR height ($R = 0.23$).

The most precise InSAR models of *H*, *G*, and *TSV* were developed using a combination of base metrics, the Mixed CHM, and textural metrics. Inclusion of metrics from the Mixed CHM resulted in the greatest gains, over the base model, for models of *H*, *G*, and *TSV*. As noted in our study the interferometric SAR height, coherence, and the CHM were previously found useful in *H* estimation (Karila et al. 2015; Persson and Fransson 2017). The best model of *TSV* relied on the Mixed CHM and its texture *mean*, as well as S_0 . Previous studies have shown the mean CHM and InSAR height to be useful for predicting *TSV* (Karila et al. 2015; Rahlf et al. 2014; Solberg et al. 2013). The gains caused by the inclusion of CHM variables were similar between both CHMs for *G* and higher when using the radar CHM for *N*. Although bivariate relationships showed textural metrics to be most strongly related to *H*, *TSV*, and *G*, and these metrics were included as top predictors within many of the best models, inclusion of textural metrics as a group resulted in little change in RF model precision for any of the four biophysical variables. Despite this ambiguity, our results suggest that textural metrics should be used for models developed from InSAR given their importance in many of the models that we constructed.

The information provided from the TanDEM-X mission proved more useful for forest estimation than past SAR data in many studies, mainly due to the use of phase height and its strong correlation to tree height and forest density (in terms of biomass or volume per hectare). However, we found that for this test site, and especially for the TanDEM-X scene that was used to generate the base metrics, the phase height exhibited a relatively weak correlation to *H* ($R = 0.46$). This may be attributable to several factors; one crucial factor is the satellite configuration – the baseline – and the height sensitivity (expressed as HOA) thereof, which was 216 m. Ideally, the HOA should be slightly larger than the tree heights to be estimated which within our study ranged from ca. 13 – 41 m. The HOA of our pair was three to seven-fold larger than most of the more precise results presented for European forests which predicted *H* with greater precision than our study (Kugler et al. 2014; Olesk et al. 2016; Persson and Fransson 2017; Soja et al. 2015a; Yu et al. 2015) but not always (Karila et al. 2015). Using five acquisitions with HOA ranging from ca. 26 – 218 m, a Canadian study within a boreal forest clearly showed the highest RMSE between the InSAR and ALS CHM was associated with an acquisition with HOA of 218 m (Sadeghi et al. 2017). In the context of these studies the relatively weak correlation that we found between phase height and *H* does appear reasonable.

The use of the Mixed CHM derived from the WorldDEM™ product and ALS data may have overcome this issue to a large extent, since the WorldDEM™ is constructed from at least two acquisitions with differing baselines. However, since this is a global product, and the processing was not optimized for the local conditions, the accuracy is usually not as high as for scenes picked and processed specifically with the purpose of forest mapping. Another potential reason for our lower precision predictions of H from phase height was the steep slopes present within the forest. This influences both the WorldDEM™ base products and the base metrics. With 97% of our plots located on slopes > 10 degrees, the long-known geometrical challenges with any SAR system play an important role. Both foreshortening, layover and shadowing effects were evident in the rasters and these effects clearly degrade the estimates as well. Since X-band mainly interacts with the top of the canopy, and the trees grow vertically and smoothen the ground slope effects, we would hope that InSAR would still be suitable in terrain with steep slopes, which is supported by the invariance of our InSAR model predictions to slope.

The results from this study clearly demonstrated the limitations of the DTM and DSM derived from InSAR at greater slopes. Most studies that have evaluated the precision of WorldDEM™ products have been undertaken in reference areas that were generally homogeneous (e.g. unbuilt areas or locations with flat uniform vegetation) and RMSE values from these studies were within the target relative vertical accuracy of 2 m (Becek et al. 2016; Cranston et al. 2018; Koppe et al. 2015). Fernandez-Diaz et al. (2018) recently extended these studies to quantify the effects of vegetation heights and terrain slope on the WorldDEM™ using ALS data as a baseline for comparison. Their study found the DSM and DTM to have mean respective RMSE values of 5.30 and 8.41 m which were similar to our mean RMSE values of, respectively, 4.58 and 8.09 m. While their results allowed differentiation of RMSE between vegetation areas with low slopes ($< 20^\circ$) and high slopes ($> 20^\circ$), our study extended this analysis to a greater slope range showing RMSE increases for the DSM and DTM to values of respectively 6.02 and 10.17 m, on slopes ranging from $40 - 50^\circ$. Although errors reported in this study were generally within the 10 m absolute vertical accuracy target set by WorldDEM™ they did slightly exceed this target on the steepest slopes. The lack of precision in these surfaces clearly limited the precision of the CHM derived solely from InSAR and highlighted the utility of using ALS to create a mixed CHM which had considerably higher mean precision than the Radar CHM (5.95 vs. 11.11m) and was markedly more useful for predicting H and TSV .

Results from this study are likely to be conservative as this study was undertaken over a forest with very steep terrain and, as previously discussed, the HOA was not optimised during image acquisition. Further research should investigate if precision gains in predictions of inventory variables are possible under acquisitions with optimised HOA. Predictions could also be improved through using an ascending and descending stereo pair to derive a DSM in which the effect of slope is minimized.

However, even if further improvements are not possible the precision demonstrated within this study highlights the potential of InSAR as a valuable means of acquiring terrain and inventory information within temperate plantations. InSAR is markedly less expensive than ALS (NZ \$0.16/ha vs. \$3 – 15/ha) and does not suffer from many of the disadvantages of ALS that include lengthy turn-around times due to flight delays, provider scheduling conflicts, and long processing times. Satellite based photogrammetric point clouds are also widely researched for forest inventory purposes and within our study forest predicted the four biophysical variables with a similar precision to ALS (Pearse et al. 2018). However, InSAR is less expensive than this data source and does not require cloud free conditions for acquisition. Furthermore, while InSAR can be used to produce a DTM, photogrammetric point clouds do not have sufficient penetration to create a DTM over forested area and this data source can only be used to precisely predict biophysical variables if a previously acquired DTM is available. Consequently, there may be instances when the advantages of InSAR outweigh the greater precision afforded by ALS and photogrammetric point clouds. Forest managers should take all of these factors into consideration when deciding on the best remote sensing approach for acquiring terrain and forest inventory information for their plantations.

Recommendations and conclusions

Models were developed for the biophysical variables *H*, *G*, *N*, and *TSV* in a temperate forest with rugged terrain using ALS and InSAR predictive metrics. The ALS models were found to be more precise and less biased than the InSAR models. Despite this, the models of *H* and *TSV* created using InSAR were found to be more precise than most previously reported studies and these models may have utility for management use. This study also quantified the precision of the CHM created from the Radar DSM and either the Radar DTM or ALS DTM. The precision of the Radar DTM and DSM, and to a lesser extent the Radar CHM, deteriorated with increasing stand slope. The integration of the ALS DTM allowed construction of a Mixed CHM which had lower error than the Radar CHM, and with the exception of the model of *N*, was a more important predictor of biophysical variables.

The precision demonstrated within this study highlights the potential of InSAR as a valuable means of supplying an inexpensive DTM and a reasonably precise means of predicting inventory metrics, particularly if data can be used in combination with a previously generated ALS DTM. InSAR is markedly less expensive than ALS (\$0.16/ha vs. \$3 – 15/ha) and does not have many of the other disadvantages of ALS that include lengthy turn-around times due to flight delays, provider scheduling conflicts, and long processing times. Compared to the use of satellite based photogrammetric point clouds, which for the forest in our study has been found to have similar precision to ALS (Pearse et al. 2018), InSAR is less expensive, does not require cloud free conditions and is unaffected by solar illumination conditions. Furthermore, while InSAR can be used to produce a DTM, satellite based photogrammetric point clouds do not have sufficient penetration to create a DTM and this data source can only be used to precisely predict biophysical variables if a previously acquired DTM is available.

Although this research does show predictions of inventory variables from InSAR to be less precise than from ALS and the use of satellite based photogrammetry there may be instances where the lower cost of InSAR is a more important consideration than the greater precision afforded by these other two methods. Forest managers should take all of these factors into consideration when deciding on the best remote sensing approach for acquiring terrain and inventory information for their plantations. We recommend further research into InSAR as an inventory tool that focusses on optimising the acquisition settings as this is likely to result in gains in the precision with which this data source can predict inventory metrics.

Acknowledgements

This study was funded by the New Zealand Forest Growers Levy Trust. Additional support for the ALS data capture was provided by Land Information New Zealand (LINZ). We are also grateful to Aaron Gunn and Port Blakely for providing access to the forest and associated inventory data.

References

- Abdullahi, S., Kugler, F., & Pretzsch, H. (2016). Prediction of stem volume in complex temperate forest stands using TanDEM-X SAR data. *Remote Sensing of Environment*, 174, 197-211
- Askne, J., Fransson, J., Santoro, M., Soja, M., & Ulander, L. (2013). Model-based biomass estimation of a hemi-boreal forest from multitemporal TanDEM-X acquisitions. *Remote Sensing*, 5, 5574-5597
- Askne, J.I., Dammert, P.B., Ulander, L.M., & Smith, G. (1997). C-band repeat-pass interferometric SAR observations of the forest. *IEEE Transactions on Geoscience and Remote Sensing*, 35, 25-35
- Askne, J.I., & Santoro, M. (2015). On the estimation of boreal forest biomass from TanDEM-X data without training samples. *IEEE Geoscience and remote sensing letters*, 12, 771-775
- Askne, J.I., Soja, M.J., & Ulander, L.M. (2017). Biomass estimation in a boreal forest from TanDEM-X data, lidar DTM, and the interferometric water cloud model. *Remote Sensing of Environment*, 196, 265-278
- Becek, K., Koppe, W., & Kutoğlu, Ş. (2016). Evaluation of vertical accuracy of the WorldDEM™ using the runway method. *Remote Sensing*, 8, 934
- Breiman, L. (2001). Random forests. *Machine learning*, 45, 5-32
- Chen, H., Cloude, S.R., & Goodenough, D.G. (2016). Forest canopy height estimation using Tandem-X coherence data. *IEEE Journal of Selected Topics in Applied Earth Observations and Remote Sensing*, 9, 3177-3188
- Cranston, J., Kariyeva, J., Roy, M., & Touzi, R. (2018). ABMI Geospatial Centre Research Team (Edmonton): Evaluation of WorldDEM DEM. In: Version 2018-04-18. Edmonton, Alberta, Canada
- Dash, J.P., Marshall, H.M., & Rawley, B. (2015). Methods for estimating multivariate stand yields and errors using k-NN and aerial laser scanning. *Forestry*
- Dobson, M.C., Ulaby, F.T., LeToan, T., Beaudoin, A., Kasischke, E.S., & Christensen, N. (1992). Dependence of radar backscatter on coniferous forest biomass. *IEEE Transactions on Geoscience and Remote Sensing*, 30, 412-415
- Fernandez-Diaz, J.C., Lee, H., & Shrestha, R.L. (2018). Evaluating the effects of Vegetation Height and Slope on the Vertical Accuracy of the Tandem-X worldDEM rapid city sample tile. In, *IGARSS 2018-2018 IEEE International Geoscience and Remote Sensing Symposium* (pp. 224-227): IEEE
- Fransson, J. (1999). Estimation of stem volume in boreal forests using ERS-1 C-and JERS-1 L-band SAR data. *International Journal of Remote Sensing*, 20, 123-137
- Frey, O., Santoro, M., Werner, C.L., & Wegmüller, U. (2012). DEM-based SAR pixel-area estimation for enhanced geocoding refinement and radiometric normalization. *IEEE Geoscience and remote sensing letters*, 10, 48-52
- Gama, F.F., Dos Santos, J.R., & Mura, J.C. (2010). Eucalyptus biomass and volume estimation using interferometric and polarimetric SAR data. *Remote Sensing*, 2, 939-956
- GDAL/OGR contributors (2019). GDAL/OGR Geospatial Data Abstraction software Library. *Open Source Geospatial Foundation*
- Goldstein, R.M., & Werner, C.L. (1998). Radar interferogram filtering for geophysical applications. *Geophysical Research Letters*, 25, 4035-4038
- Goodbody, T.R., Coops, N.C., & White, J.C. (2019). Digital Aerial Photogrammetry for Updating Area-Based Forest Inventories: A Review of Opportunities, Challenges, and Future Directions. *Current Forestry Reports*, 1-21
- Hansen, E.H., Gobakken, T., Solberg, S., Kangas, A., Ene, L., Mauya, E., & Næsset, E. (2015). Relative efficiency of ALS and InSAR for biomass estimation in a Tanzanian rainforest. *Remote Sensing*, 7, 9865-9885
- Holmgren, J. (2004). Prediction of tree height, basal area and stem volume in forest stands using airborne laser scanning. *Scandinavian Journal of Forest Research*, 19, 543-553
- Karila, K., Vastaranta, M., Karjalainen, M., & Kaasalainen, S. (2015). Tandem-X interferometry in the prediction of forest inventory attributes in managed boreal forests. *Remote Sensing of Environment*, 159, 259-268
- Karila, K., Yu, X., Vastaranta, M., Karjalainen, M., Puttonen, E., & Hyypä, J. (2019). TanDEM-X digital surface models in boreal forest above-ground biomass change detection. *ISPRS journal of photogrammetry and remote sensing*, 148, 174-183

- Khosravipour, A., Skidmore, A.K., Isenburg, M., Wang, T., & Hussin, Y.A. (2014). Generating pit-free canopy height models from airborne lidar. *Photogrammetric Engineering & Remote Sensing*, 80, 863-872
- Koppe, W., Henrichs, L., & Hummel, P. (2015). Assessment of WorldDEM TM global elevation model using different references. In, *2015 IEEE International Geoscience and Remote Sensing Symposium (IGARSS)* (pp. 5296-5299): IEEE
- Krieger, G., Moreira, A., Fiedler, H., Hajnsek, I., Werner, M., Younis, M., & Zink, M. (2007). TanDEM-X: A satellite formation for high-resolution SAR interferometry. *IEEE Transactions on Geoscience and Remote Sensing*, 45, 3317-3341
- Kugler, F., Schulze, D., Hajnsek, I., Pretzsch, H., & Papathanassiou, K.P. (2014). TanDEM-X Pol-InSAR performance for forest height estimation. *IEEE Transactions on Geoscience and Remote Sensing*, 52, 6404-6422
- Lavalle, M., & Hensley, S. (2015). Extraction of structural and dynamic properties of forests from polarimetric-interferometric SAR data affected by temporal decorrelation. *IEEE Transactions on Geoscience and Remote Sensing*, 53, 4752-4767
- Le Toan, T., Beaudoin, A., Riou, J., & Guyon, D. (1992). Relating forest biomass to SAR data. *IEEE Transactions on Geoscience and Remote Sensing*, 30, 403-411
- Lee, S.-K., Kugler, F., Papathanassiou, K.P., & Hajnsek, I. (2013). Quantification of temporal decorrelation effects at L-band for polarimetric SAR interferometry applications. *IEEE Journal of Selected Topics in Applied Earth Observations and Remote Sensing*, 6, 1351-1367
- Massonnet, D., & Feigl, K.L. (1998). Radar interferometry and its application to changes in the Earth's surface. *Reviews of geophysics*, 36, 441-500
- Moreira, A., Prats-Iraola, P., Younis, M., Krieger, G., Hajnsek, I., & Papathanassiou, K.P. (2013). A tutorial on synthetic aperture radar. *IEEE Geoscience and Remote Sensing Magazine*, 1, 6-43
- Neeff, T., Dutra, L.V., dos Santos, J.R., Freitas, C.d.C., & Araujo, L.S. (2005). Tropical forest measurement by interferometric height modeling and P-band radar backscatter. *Forest Science*, 51, 585-594
- NZFOA (2018). Facts and Figures 2017/2018. New Zealand Forest Owners Association, Wellington, 60 pp
- Olesk, A., Praks, J., Antropov, O., Zalite, K., Arumäe, T., & Voormansik, K. (2016). Interferometric SAR coherence models for characterization of hemiboreal forests using TanDEM-X Data. *Remote Sensing*, 8, 700
- Pearse, G.D., Dash, J.P., Persson, H.J., & Watt, M.S. (2018). Comparison of high-density LiDAR and satellite photogrammetry for forest inventory. *ISPRS journal of photogrammetry and remote sensing*, 142, 257-267
- Pedregosa, F., Varoquaux, G., Gramfort, A., Michel, V., Thirion, B., Grisel, O., Blondel, M., Prettenhofer, P., Weiss, R., Dubourg, V., Vanderplas, J., Passos, A., Cournapeau, D., Brucher, M., Perrot, M., & Duchesnay, E. (2011). Scikit-learn: Machine Learning in Python. *Journal of Machine Learning Research*, 12, 2825-2830
- Perko, R., Raggam, H., Deutscher, J., Gutjahr, K., & Schardt, M. (2011). Forest assessment using high resolution SAR data in X-band. *Remote Sensing*, 3, 792-815
- Persson, H., Olsson, H., Soja, M., Ulander, L., & Fransson, J. (2017). Experiences from large-scale forest mapping of Sweden using TanDEM-X data. *Remote Sensing*, 9, 1253
- Persson, H.J. (2016). Estimation of Boreal Forest Attributes from Very High Resolution Pléiades Data. *Remote Sensing*, 8
- Persson, H.J., & Fransson, J.E. (2017). Comparison between TanDEM-X and ALS-based estimation of aboveground biomass and tree height in boreal forests. *Scandinavian Journal of Forest Research*, 32, 306-319
- Puliti, S., Solberg, S., Næsset, E., Gobakken, T., Zahabu, E., Mauya, E., & Malimbwi, R. (2017). Modelling above ground biomass in Tanzanian miombo woodlands using TanDEM-X WorldDEM and field data. *Remote Sensing*, 9, 984
- Qi, W., Lee, S.-K., Hancock, S., Luthcke, S., Tang, H., Armston, J., & Dubayah, R. (2019). Improved forest height estimation by fusion of simulated GEDI Lidar data and TanDEM-X InSAR data. *Remote Sensing of Environment*, 221, 621-634
- R. Core Team (2019). *R: A Language and Environment for Statistical Computing*. Vienna, Austria: R Foundation for Statistical Computing
- Rahlf, J., Breidenbach, J., Solberg, S., Næsset, E., & Astrup, R. (2014). Comparison of four types of 3D data for timber volume estimation. *Remote Sensing of Environment*, 155, 325-333
- Rignot, E., Way, J., Williams, C., & Viereck, L. (1994). Radar estimates of aboveground biomass in boreal forests of interior Alaska. *IEEE Transactions on Geoscience and Remote Sensing*, 32, 1117-1124

- Sadeghi, Y., St-Onge, B., Leblon, B., & Simard, M. (2017). Effects of TanDEM-X Acquisition Parameters on the Accuracy of Digital Surface Models of a Boreal Forest Canopy. *Canadian Journal of Remote Sensing*, 43, 194-207
- Schlund, M., Baron, D., Magdon, P., & Erasmi, S. (2019). Canopy penetration depth estimation with TanDEM-X and its compensation in temperate forests. *ISPRS journal of photogrammetry and remote sensing*, 147, 232-241
- Shang, C., Treitz, P., Caspersen, J., & Jones, T. (2019). Estimation of forest structural and compositional variables using ALS data and multi-seasonal satellite imagery. *International Journal of Applied Earth Observation and Geoinformation*, 78, 360-371
- Small, D. (2011). Flattening gamma: Radiometric terrain correction for SAR imagery. *IEEE Transactions on Geoscience and Remote Sensing*, 49, 3081-3093
- Soja, M.J., Persson, H., & Ulander, L.M. (2015a). Estimation of forest height and canopy density from a single InSAR correlation coefficient. *IEEE Geoscience and remote sensing letters*, 12, 646-650
- Soja, M.J., Persson, H.J., & Ulander, L.M. (2015b). Estimation of forest biomass from two-level model inversion of single-pass InSAR data. *IEEE Transactions on Geoscience and Remote Sensing*, 53, 5083-5099
- Solberg, S., Astrup, R., Breidenbach, J., Nilsen, B., & Weydahl, D. (2013). Monitoring spruce volume and biomass with InSAR data from TanDEM-X. *Remote Sensing of Environment*, 139, 60-67
- Solberg, S., Hansen, E.H., Gobakken, T., Næssset, E., & Zahabu, E. (2017). Biomass and InSAR height relationship in a dense tropical forest. *Remote Sensing of Environment*, 192, 166-175
- Stone, C., Penman, T.D., & Turner, R. (2011). Determining an optimal model for processing lidar data at the plot level: results for a *Pinus radiata* plantation in New South Wales, Australia
- Treuhäft, R., Gonçalves, F., Dos Santos, J.R., Keller, M., Palace, M., Madsen, S.N., Sullivan, F., & Graça, P.M. (2015). Tropical-forest biomass estimation at X-band from the spaceborne TanDEM-X interferometer. *IEEE Geoscience and remote sensing letters*, 12, 239-243
- Watt, M.S., Palmer, D.J., & Höck, B.K. (2011). Spatial description of potential areas suitable for afforestation within New Zealand and quantification of their productivity under *Pinus radiata*. *New Zealand Journal of Forestry Science*, 41, 115-129
- Wegmüller, U., Werner, C., Strozzi, T., & Wiesmann, A. (2002). Phase unwrapping with GAMMA ISP technical report, 13-May-2002. *Gamma Remote Sensing: Bern, Switzerland*
- Wessel, B. (2016). TanDEM-X Ground Segment–DEM Products Specification Document, EOC, DLR, Oberpfaffenhofen, Germany, Public Document TD-GS-PS-0021, Issue 3.1. In
- Wittke, S., Yu, X., Karjalainen, M., Hyypä, J., & Puttonen, E. (2019). Comparison of two-dimensional multitemporal Sentinel-2 data with three-dimensional remote sensing data sources for forest inventory parameter estimation over a boreal forest. *International journal of applied earth observation and geoinformation*, 76, 167-178
- Yu, X., Hyypä, J., Karjalainen, M., Nurminen, K., Karila, K., Vastaranta, M., Kankare, V., Kaartinen, H., Holopainen, M., & Honkavaara, E. (2015). Comparison of laser and stereo optical, SAR and InSAR point clouds from air-and space-borne sources in the retrieval of forest inventory attributes. *Remote Sensing*, 7, 15933-15954
- Zink, M., Fiedler, H., Hajnsek, I., Krieger, G., Moreira, A., & Werner, M. (2006). The TanDEM-X mission concept. In, *2006 IEEE International Symposium on Geoscience and Remote Sensing* (pp. 1938-1941): IEEE
- Zvoleff, A. (2019). *glcm: Calculate Textures from Grey-Level Co-Occurrence Matrices (GLCMs)*.

Appendix A

Summary statistics for Radar variables classified under four categories: base metrics, CHMs, and textural metrics derived from the Mixed CHM and Radar CHM. Shown are the mean, standard deviation (SD) and the range from 171 plots.

| Variable | Abbrev. | Mean | SD | Range |
|---|----------------------|-------|------|---------------|
| Base Metrics | | | | |
| Phase Height | PH | 16.3 | 6.46 | 0.93 – 49.5 |
| Phase Height Standard Deviation | PH SD | 3.24 | 2.03 | 1.06 – 15.0 |
| Corrected Coherence | COH CORR | 0.85 | 0.08 | 0.44 – 0.95 |
| Local Incidence Angle | INC | 0.79 | 0.26 | 0.14 – 1.27 |
| Radar Backscatter | S0 | -11.6 | 1.74 | -16.7 – -6.62 |
| Canopy Height Models (CHM) | | | | |
| CHM derived from Radar DSM and ALS DTM | Mixed CHM | 15.9 | 5.99 | 2.05 – 31.0 |
| CHM derived from Radar DSM and Radar DTM | Radar CHM | 9.92 | 2.44 | 0.10 – 17.4 |
| Textural Metrics derived using Mixed CHM | | | | |
| <i>Contrast</i> | <i>Contrast</i> | 6.88 | 5.01 | 1.17 – 30.4 |
| <i>Correlation</i> | <i>Correlation</i> | 0.31 | 0.22 | -0.25 – 0.88 |
| <i>Dissimilarity</i> | <i>Dissimilarity</i> | 1.93 | 0.69 | 0.79 – 4.41 |
| <i>Entropy</i> | <i>Entropy</i> | 2.02 | 0.13 | 1.53 – 2.18 |
| <i>Homogeneity</i> | <i>Homogeneity</i> | 0.41 | 0.10 | 0.18 – 0.65 |
| <i>Mean</i> | <i>Mean</i> | 0.37 | 0.13 | 0.11 – 0.69 |
| <i>Second Moment</i> | <i>Sec. moment</i> | 0.14 | 0.03 | 0.11 – 0.28 |
| <i>Variance</i> | <i>Variance</i> | 151 | 92.4 | 12.1 – 470 |
| Textural Metrics derived using Radar CHM | | | | |
| <i>Contrast</i> | <i>Contrast</i> | 5.15 | 4.55 | 0.58 – 28.5 |
| <i>Correlation</i> | <i>Correlation</i> | 0.20 | 0.19 | -0.24 – 0.79 |
| <i>Dissimilarity</i> | <i>Dissimilarity</i> | 1.58 | 0.70 | 0.41 – 4.06 |
| <i>Entropy</i> | <i>Entropy</i> | 1.88 | 0.22 | 0.99 – 2.20 |
| <i>Homogeneity</i> | <i>Homogeneity</i> | 0.49 | 0.12 | 0.20 – 0.81 |
| <i>Mean</i> | <i>Mean</i> | 0.28 | 0.05 | 0.05 – 0.46 |
| <i>Second Moment</i> | <i>Sec. moment</i> | 0.17 | 0.05 | 0.11 – 0.45 |
| <i>Variance</i> | <i>Variance</i> | 80.8 | 26.5 | 3.36 – 206 |

Appendix B

Summary statistics for ALS variables classified under three categories: base metrics, CHMs, and textural metrics. Shown are the mean, standard deviation (SD) and the range from 171 plots.

| Variable | Abbrev. | Mean | SD | Range |
|---|----------------------|-------|------|--------------|
| Base metrics | | | | |
| Maximum height | Max Height | 35.3 | 5.07 | 16.4 – 46.6 |
| Mean height | Mean Height | 14.6 | 3.71 | 3.30 – 21.9 |
| Quadratic mean height | Quadratic M | 17.3 | 3.72 | 4.35 – 24.6 |
| Standard Deviation of height | SD | 9.16 | 1.57 | 2.83 – 12.4 |
| Skewness of height values | Skew | -0.17 | 0.53 | -1.39 – 1.92 |
| Kurtosis of height values | Kurtosis | 2.21 | 0.66 | 1.45 – 6.21 |
| Coefficient of variation | CV | 0.66 | 0.17 | 0.41 – 1.37 |
| Mid-point of most frequent 1 m bin from a histogram of points > 1.4 m | Mode | 17.4 | 8.16 | 1.50 – 28.5 |
| Height of quantile h | p99.5 | 32.2 | 4.84 | 12.8 – 42.3 |
| | p99 | 31.2 | 4.76 | 12.0 – 41.0 |
| | p95 | 28.1 | 4.56 | 9.08 – 37.4 |
| | p90 | 26.0 | 4.60 | 7.18 – 34.6 |
| | p75 | 21.7 | 5.05 | 4.02 – 29.9 |
| | p50 | 15.7 | 5.02 | 1.26 – 24.2 |
| | p25 | 7.38 | 4.60 | 0.16 – 20.0 |
| Canopy density metrics at h% of height | b99 | 99.2 | 0.09 | 98.7 – 99.4 |
| | b95 | 98.1 | 0.41 | 96.7 – 99.0 |
| | b90 | 95.6 | 1.24 | 91.3 – 98.4 |
| | b80 | 86.4 | 4.43 | 70.9 – 96.8 |
| | b75 | 79.9 | 6.43 | 57.3 – 95.6 |
| | b50 | 43.2 | 13.8 | 9.77 – 90.5 |
| | b25 | 17.3 | 13.6 | 1.90 – 74.5 |
| | b10 | 8.51 | 10.4 | 0.53 – 65.7 |
| Canopy cover as number of 1st returns > h/total 1st returns | CCov DBH | 90.6 | 8.69 | 47.9 – 99.5 |
| | CCov 5m | 83.3 | 15.2 | 25.6 – 97.7 |
| | CCov 10m | 76.1 | 18.0 | 4.51 – 96.8 |
| Vertical complexity index (1 m bins) | VCI | 0.85 | 0.06 | 0.58 – 0.94 |
| Canopy Height Models (CHM) | | | | |
| Maximum height of CHM pixels | CHM Max | 34.3 | 5.06 | 13.7 – 44.7 |
| Average height of CHM pixels | CHM Mean | 20.0 | 5.01 | 5.06 – 30.5 |
| Median value of CHM pixels | CHM Median | 20.9 | 6.07 | 2.26 – 30.5 |
| Standard Deviation of CHM pixels | CHM SD | 7.37 | 2.03 | 2.90 – 13.0 |
| Height of quantile h of CHM pixels | CHM p99 | 32.4 | 4.88 | 12.7 – 42.3 |
| | CHM p95 | 30.3 | 4.68 | 11.0 – 39.9 |
| | CHM p90 | 28.7 | 4.69 | 9.48 – 38.2 |
| | CHM p75 | 25.5 | 5.35 | 6.66 – 34.6 |
| | CHM p50 | 20.9 | 6.07 | 2.26 – 30.5 |
| | CHM p25 | 15.1 | 6.35 | 0.12 – 26.8 |
| Textural metrics | | | | |
| <i>Contrast</i> | <i>Contrast</i> | 8.94 | 3.86 | 0.98 – 20.1 |
| <i>Correlation</i> | <i>Correlation</i> | 0.56 | 0.05 | 0.39 – 0.68 |
| <i>Dissimilarity</i> | <i>Dissimilarity</i> | 2.06 | 0.49 | 0.63 – 3.30 |
| <i>Entropy</i> | <i>Entropy</i> | 1.94 | 0.17 | 1.27 – 2.12 |
| <i>Homogeneity</i> | <i>Homogeneity</i> | 0.42 | 0.08 | 0.28 – 0.72 |
| <i>Mean</i> | <i>Mean</i> | 0.46 | 0.11 | 0.13 – 0.70 |
| <i>Second Moment</i> | <i>Sec. moment</i> | 0.17 | 0.05 | 0.13 – 0.42 |
| <i>Variance</i> | <i>Variance</i> | 244 | 91.6 | 19.9 – 479 |